DTIC FILE COPY

AD-A229 504

A/U OF DAYTON PHOTOREFRACTIVE BEAM TRACKING

University of Dayton

Grame Duthie and H.J. Caulfield

DTIC
ELECTE
NOV 30 1990
S B D

90

This report has been reviewed by the RADC Public Affairs Division (PA) and is releasable to the National Technical Information Services (NTIS) At NTIS it will be releasable to the general public, including foreign nations.

RADC-TR-90-254 has been reviewed and is approved for publication.
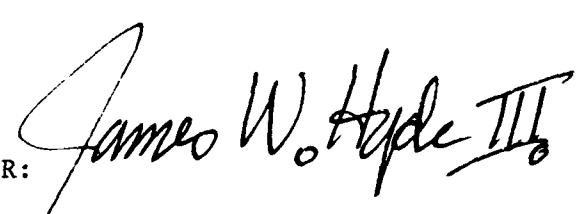
APPROVED:

DAVID A. CORDEIRO
Project Engineer

APPROVED:

FRANCIS G. REID, Colonel, USAF
Director of Communications

FOR THE COMMANDER:

JAMES W. HYDE III
Directorate of Plans & Programs

REPORT DOCUMENTATION PAGE

Public reporting burden for this collection of information is estimated to average 1 hour per response, including the time for reviewing instructions, searching existing data sources, gathering and maintaining the data needed, and completing and reviewing the collection of information. Send comments regarding the burden estimate or any other aspect of this collection of information, including suggestions for reducing this burden, to Washington Headquarters Services, Directorate for Information Operations and Reports, 1215 Jefferson Davis Highway, Suite 1204, Arlington, VA 22202-4302, and to the Office of Management and Budget, Paperwork Reduction Project (0704-0188), Washington, DC 20503.

1. AGENCY USE ONLY (Leave Blank)	2. REPORT DATE October 1990	3. REPORT TYPE AND DATES COVERED Final Feb 89 - Feb 90

4. TITLE AND SUBTITLE
A/U OF DAYTON PHOTOREFRACTIVE BEAM TRACKING

6. AUTHOR(S)
Grame Duthie, H. J. Caulfield

5. FUNDING NUMBERS
C - F30602-88-D-0028
PE - 63726F
PR - 2863
TA - 92
WU - PF

7. PERFORMING ORGANIZATION NAME(S) AND ADDRESS(ES)

University of Alabama
Center for Applied Optics, Research Institute E12
Huntsville AL 35899

8. PERFORMING ORGANIZATION REPORT NUMBER

9. SPONSORING/MONITORING AGENCY NAME(S) AND ADDRESS(ES)

Rome Air Development Center (DCLW)
Griffiss AFB NY 13441-5700

10. SPONSORING/MONITORING AGENCY REPORT NUMBER

RADC-TR-90-254

11. SUPPLEMENTARY NOTES
RADC Project Engineer: David A. Cordeiro/DCLW/(315) 330-4092
The prime contractor for this effort was University of Dayton, 300 College Park KL-262, Dayton OH 45469.

12a. DISTRIBUTION/AVAILABILITY STATEMENT

Approved for public release; distribution unlimited.

12b. DISTRIBUTION CODE

13. ABSTRACT (Maximum 200 words)
This report explains the properties of Barium Titanate being used for communication applications. Research was done dealing with steady state and transient behavior of several double phase conjugate mirror systems. This included both theoretical modeling and experimental testing verification.

14. SUBJECT TERMS
Photorefractive Materials, Phase Conjugation

15. NUMBER OF PAGES
84

16. PRICE CODE

17. SECURITY CLASSIFICATION OF REPORT	18. SECURITY CLASSIFICATION OF THIS PAGE	19. SECURITY CLASSIFICATION OF ABSTRACT	20. LIMITATION OF ABSTRACT
UNCLASSIFIED	UNCLASSIFIED	UNCLASSIFIED	UL

NSN 7540-01-280-5500

Standard Form 298 (Rev. 2-89)
Prescribed by ANSI Std. Z39-18
298-102

Preface

During the funding period we performed research on the photorefractive properties of Barium Titanate. We were particularly interested in communications applications of double phase conjugate mirrors. We performed research into the steady state and transient behavior of several double phase conjugate mirror systems. This included both theoretical modeling and experimental testing and verification. In the process of the work we invented a new architecture for photorefractive phase conjugation — the Semi—Linear Double Phase Conjugate mirror which is simple to operate, is somewhat faster than conventional double phase conjugation and which can show significant gain in the conjugated beam.

2.   Introduction to Photorefractive Double Phase Conjugation

A very fine review of the photorefractive properties of materials such as Barium Titanate with respect to four wave mixing is given by J. Feinberg in the book "Four Wave Mixing", by Robert Fisher. The process depends on the formation of holographic gratings in polled crystalline $BaTiO_3$ through the photorefractive effect and subsequent read—out of these holograms by a suitable laser beam. The reader is referred to that text as prerequisite reading for this report.

Photorefractive Mutually Pumped Phase Conjugate (MPPC) is the process in which two phase conjugate wavefronts are simultaneously generated by two mutually incoherent laser beams in photorefractive materials. There are three interesting properties of MPPC. First, the two pump beams can be temporally incoherent or even with different wavelength in some configuration. Secondly, the two pumping waves are actually exchanging their spatial wavefront in a phase conjugate way during the process. Finally, no spatial and temporal modulation cross—talk have been observed in the output beams. These unusual characteristics of MPPC make it very attraction in various applications, which are going to be discussed in section 5.

3. Basic Mechanism of Mutually Pumped Phase Conjugators

In recent years, several configurations of mutually pumped phase conjugators (MPPC), as shown in Figure (3.1) and (3.2), have been proposed and demonstrated experimentally. The Double Phase Conjugate Mirror (DPCM) was first proposed and theoretically studied by Cronin–Golomb et al.[1] and was demonstrated experimentally by Weiss et al. in 1987.[2] The Mutually Incoherent Beam Coupler (MIBC) and Bird–Wing Phase Conjugator (BWPC) were soon introduced by Smout et al.[3] and Ewbank[4], respectively. In this section we are going to discuss the basic mechanism of MPPC, introduce a two–interactive region model[5] for studying the intensity performances of one class of MPPC and compare our theory with the experiment. We also introduce and present experimental results on a new configuration[7] of MPPC interaction which we call the Semilinear Double Phase Conjugates Mirror (SDPCM).

How do two mutually incoherent mixed beams generate a pair of phase conjugate wavefronts in photorefractive materials? This question has been addressed by several authors.[4,8] The mechanism is not difficult to understand in terms of four–wave mixing with a transmission type of grating. Taking the Double Phase Conjugate Mirror (DPCM), as an example, which was first proposed by Cronin–Golomb et al.[1] and experimentally demonstrated by Weiss et al.,[2] the four–wave mixing process can be characterized by the coupled wave equations, Eq. (1), Fig. (3.2). The transmission grating is formed by the interference patter of $A_1A_4^* + A_2^*A_3$ where $\vec{k}_2 - \vec{k}_3 = \vec{k}_4 - \vec{k}_1$. Obviously, for the transmission grating process, it is not necessary to require all the four beams to be mutually temporally coherent except that A_1 and A_3 are coherent with A_4 and A_2, respectively. In the case of the MPPC process in the DPCM two mutually incoherent beams A_4 and A_2, respectively. In the case of the MPPC process in the DPCM two mutually incoherent beams A_4 and A_2 are incident on the crystal. As discussed in the previous chapter, the fanning beam of A_4 and A_2 result in holograms which diffract A_1 and A_3, respectively. If and only if the diffracted beams satisfy the phase matching condition,

$\vec{k}_2 - \vec{k}_3 = \vec{k}_4 - \vec{k}_1$ and the coupling strength of the material exceeds a certain threshold, the grating $A_1 A_4^* + A_2^* A_3$ will be reinforced and the self–induced oscillation can be sustained. Such an oscillation *does not necessarily* produce two phase conjugate outputs because there is an extra degree of freedom for the oscillating wave vectors satisfying the phase conjugation requirement, $\vec{k}_1 = -\vec{k}_2$ and $\vec{k}_3 = -\vec{k}_4$. This extra degree of freedom often causes off–plane conical scattering especially in the configuration like DPCM where only one interactive region exists. However, it is noticed that the oscillation process usually selects the "spatial mode" which has the highest gain. In the process of MPPC, the spatial mode experiencing the highest gain is the "mode" in which oscillating beams have the *maximum spatial overlap* with respect to their incident beams, i.e., they are phase conjugate pairs.[6] Such a "spatial mode competition" process eliminates the ambiguity of oscillating wave vectors forcing the conical scattering to collapse into the well defined phase conjugate output. This is more effective when the incident beams are spatially modulated.

As seen in Fig. (3.2), MPPC may be divided into two categories: one–region process and two–region process. DPCM has been analyzed by four–wave mixing in one interactive region model. However, MIBC and BWPC are apparently involved in the interaction of two coupled interactive regions. Therefore, we introduce the two–interactive region model for MPPC.

BWPC and MIBC are both two–interactive–region processes. The schematic diagrams for this class of four–wave mixing are shown in Fig. (3.2). Two mutually incoherent beams, A_4 and A_2', are incident on the photorefractive crystal, beams A_1 and A_3' are diffracted from A_4 and A_2', respectively, by their fanning holograms. These are then internally reflected by the surfaces of the crystal (one reflection for BWPC and two reflections for MIBC) becoming A_4' and A_2, respectively. If and only if A_4' and A_2 are phase conjugate with A_3' and A_1, respectively, two sets of gratings, $A_1 A_4^* + A_2^* A_3$ and $A_1' A_4'^* + A_2'^* A_3'$, will be reinforced by these beams. All other fanning holograms decay gradually.

4

Mathematically, we start from the typical four-wave mixing equations in the two separate regions. The diffusion dominated photorefractive effect is considered here since this is the most useful and practical situation for applications. Due to the $\pi/2$ phase shift between the interference pattern and the index grating in these cases, the photorefractive coupling coefficient γ_i are real constants. Therefore, we may use the intensity equations[9],[10] instead of complex amplitude equations, Eq. (1), to study the problem.

$$\frac{dA_1}{dz} = \frac{\gamma}{I_0}(A_1 A_4^* + A_2^* A_3)A_4 - \alpha A_1$$

$$\frac{dA_2^*}{dz} = \frac{\gamma}{I_0}(A_1 A_4^* + A_2^* A_3)A_2 + \alpha A_2^*$$

$$\frac{dA_3}{dz} = -\frac{\gamma}{I_0}(A_1 A_4^* + A_2^* A_3)A_1^* - \alpha A_4^*$$

$$\frac{dA_4^*}{dz} = -\frac{\gamma}{I_0}(A_1 A_4^* + A_2^* A_3)A_1^* - \alpha A_4^* \qquad (1)$$

where $A_i (i = 1 \approx 4)$ are the slowly varying complex amplitudes of light beams, and

$$I_0 = |A_1|^2 + |A_2|^2 + |A_3|^2 + |A_4|^2.$$

For region I:

$$\frac{dI_1}{dz} = -\alpha I_1 + \gamma_1 \left[I_1 I_4 + \sqrt{I_1 I_2 I_3 I_4} \right] / I_0 \qquad (2a)$$

$$\frac{dI_2}{dz} = +\alpha I_2 + \gamma_1 \left[I_2 I_3 + \sqrt{I_1 I_2 I_3 I_4} \right] / I_0 \qquad (2b)$$

$$\frac{dI_3}{dz} = +\alpha I_3 - \gamma_1 \left[I_2 I_3 + \sqrt{I_1 I_2 I_3 I_4} \right] / I_0 \qquad (2c)$$

$$\frac{dI_4}{dz} = -\alpha I_4 - \gamma_1 \left[I_1 I_4 + \sqrt{I_1 I_2 I_3 I_4} \right] / I_0 \tag{2d}$$

For region II:

$$\frac{dI_1'}{dz'} = -\alpha I_1' + \gamma_2 \left[I_1' I_4' + \sqrt{I_1' I_2' I_3' I_4'} \right] / I_0' \tag{2e}$$

$$\frac{dI_2'}{dz'} = \alpha I_2' + \gamma_2 \left[I_2' I_3' + \sqrt{I_1' I_2' I_3' I_4'} \right] / I_0' \tag{2f}$$

$$\frac{dI_3'}{dz'} = \alpha I_3' + \gamma_2 \left[I_2' I_3' + \sqrt{I_1' I_2' I_3' I_4'} \right] / I_0' \tag{2g}$$

$$\frac{dI_4'}{dz'} = -\alpha I_4' + \gamma_2 \left[I_1' I_4' + \sqrt{I_1' I_2' I_3' I_4'} \right] / I_0' \tag{2h}$$

where

$$I_0 = |A_1|^2 + |A_2|^2 + |A_3|^2 + |A_4|^2 \tag{3a}$$

$$I_0' = |A_1'|^2 + |A_2'|^2 + |A_3'|^2 + |A_4'|^2 \tag{3b}$$

γ_1 and γ_2 are the photorefractive coupling coefficients for region I and II, and α is the absorption coefficient. Here γ_1, γ_2 and α are twice the values in the complex amplitude equations, Eq. (1).

The boundary conditions and coupling conditions for the BWPC and MIBC are described as:

boundary conditions:

$$I_1(0) = 0; \quad I_1'(0) = 0; \quad I_3(l_1) = 0; \quad I_3'(l_2) = 0 \tag{4a}$$

incident beams:

$$I_4(0) = 1; \quad I_2'(l_2) = q \tag{4b}$$

coupling conditions:

$$I_2(l_1) = RI_3'(0)e^{-\alpha d}$$

$$I_4'(0) = RI_1(l_1)e^{-\alpha d} \tag{4c}$$

where $R = 1 - L$, L is the loss due to imperfect internal reflection, d is the distance between these two regions, q is the input beam ration of $I_2'(l_2)/I_4(0)$, l_1 and l_2 are the interaction lengths of the two regions.

We use the method developed by Belic[9],[10] to solve the coupled eqautions (2a–h). After some manipulations, we obtain the following expressions for all the intensities in terms of parameters Y, Y' and auxiliary functions $y(z)$ and $y'(z')$.

$$I_1(z) = e^{-\alpha z} cos^2\left[\frac{y(z) + Y}{2}\right]$$

$$I_2(z) = qRe^{-\alpha d}e^{\alpha(z-l_1-l_2)}cos^2\left[\frac{Y'}{2}\right] cos^2\left[\frac{y(z)}{2}\right]$$

$$I_3'(z) = qRe^{-\alpha d}e^{\alpha(z-l_1-l_2)}cos^2\left[\frac{Y'}{2}\right] sin^2\left[\frac{y(z)}{2}\right]$$

$$I_4(z) = e^{-\alpha z} sin^2\left[\frac{y(z) + Y}{2}\right] \tag{5}$$

$$I_1'(z') = Re^{-\alpha d}e^{-\alpha(z'+l_1)}cos^2\left[\frac{Y}{2}\right] cos^2\left[\frac{y'(z') + Y'}{2}\right]$$

$$I_2'(z') = qe^{\alpha(z'-l_2)}cos^2\left[\frac{y'(z')}{2}\right]$$

$$I_3'(z') = qe^{\alpha(z'-l_2)}sin^2\left[\frac{y'(z')}{2}\right]$$

$$I_4'(z') = Re^{-\alpha d}e^{-\alpha(z'+l_1)}cos^2\left[\frac{Y}{2}\right]sin^2\left[\frac{y'(z') + Y'}{2}\right] \tag{6}$$

where $y(z)$ and $y'(z')$ are the two parameters Y and Y' are determined by the following differential equations with boundary conditions

$$-2\frac{dy(z)}{dz} = \frac{\gamma_1}{u_1 + u_2}[(u_1 cos Y + u_2)siny(z) + u_1 sin Y cosy(z)] \tag{7a}$$

$$-2\frac{dy'(z')}{dz'} = \frac{\gamma_2}{u_1' + u_2'}[(u_1' cos Y' + u_2')siny'(z') + u_1' sin Y' cosy'(z')] \tag{7b}$$

where

$$u_1 = e^{-\alpha z}$$

$$u_2 = qRe^{\alpha(z-l_1-l_2-d)}cos^2\left[\frac{Y'}{2}\right]$$

$$u_1' = Re^{-\alpha(z'+l_1+d)}cos^2\left[\frac{Y}{2}\right]$$

$$u_2' = qe^{\alpha(z'-l_2)} \tag{8}$$

$$y(z)|_{z=0} = \pi - Y; \quad y(z)|_{z=l_1} = 0;$$

$$y'(z')|_{z'=0} = \pi - Y'; \quad y'(z')|_{z'=l_2} = 0 \tag{9}$$

By solving Eq. (7) with boundary conditions (9), all the beam intensities in the crystal can be obtained by (5) and (6) with arbitrary coupling strengths and absorptions. If we define the phase conjugate reflectives R_1, R_2 and the coupling transmission efficiencies

8

T_1, T_2 as

$$R_1 = \frac{I_3(0)}{I_4(0)} , \quad R_2 = \frac{I_1^{'}(l_2)}{I_2(l_2)} ,$$

$$T_1 = \frac{I_1^{'}(l_2)}{I_4(0)} , \quad T_2 = \frac{I_3(0)}{I_2(l_2)} .$$

Using the intensities derived in (5), (Γ) and boundary conditions (9), we have

$$T = T_1 = T_2 = Re^{-\alpha(d+l_1+l_2)} cos^2\left[\frac{Y}{2}\right] cos^2\left[\frac{Y'}{2}\right] , \tag{10a}$$

$$R_1 = qRe^{-\alpha(d+l_1+l_2)} cos^2\left[\frac{Y}{2}\right] cos^2\left[\frac{Y'}{2}\right] , \tag{10b}$$

$$R_2 = \frac{R}{q} e^{-\alpha(d+l_1+l_2)} cos^2\left[\frac{Y}{2}\right] cos^2\left[\frac{Y'}{2}\right] , \tag{10c}$$

which satisfy the relations

$$R_1 = Tq, \quad R_2 = \frac{T}{q} .$$

These are the same as the relations obtained from the one–region model, i.e., the double phase conjugate mirror process.[1,2]

For the case of negligible absorption ($\alpha = 0$), u and u' in (8) become constants. Therefore, Eq (7) can be integrated analytically. After applying the boundary conditions given in (9) we obtain two nonlinear algebraic equations for the parameters Y and Y' as follows:

$$\cot \frac{Y - \xi}{2} = \tan\left[\frac{\xi}{2}\right] e^{2[1 + qR\cos^2(Y'/2)]^{\gamma_1 l_1}}$$

$$\sqrt{1 + 2qR\cos Y \cos^2(Y'/2 + q^2 R^2 \cos^4(Y'/2}$$
(11a)

$$\cot \frac{Y' - \eta}{2} = \tan\left[\frac{\eta}{2}\right] e^{2[q + qR\cos^2(Y/2)]^{\gamma_2 l_2}}$$

$$\sqrt{q^2 + 2qR\cos^2(Y/2)\cos Y' + R^2\cos^4(Y/2)]}$$
(11b)

where

$$\xi = \tan^{-1}\left[\frac{\sin Y}{\cos Y + qR\cos^2\left(\frac{Y}{2}\right)}\right]$$

$$\eta = \tan^{-1}\left[\frac{R\cos^2\left(\frac{Y}{2}\right)\sin Y'}{q + R\cos^2\left(\frac{Y}{2}\right)\cos Y'}\right]$$

Solving the above equations for Y and Y', we get the phase conjugate reflectivities and the coupling transmission efficiency by (10).

We not present some numerical results for these two interactive–region model without absorption ($\alpha = 0$), discuss the competition phenomena among various mechanisms and compare the performances on one–region and two–region processes. The absorption effects is also discussed in the DPCM configuration.

For the symmetric case, where the coupling strengths of the two regions are equal and the input beam intensities are equal, i.e., $\gamma_1 l_1 = \gamma_2 l_2 = \gamma l$ and $q = 1$, we know from (10) that the two phase conjugates reflectivities R_1, R_2 and the coupling transmission efficiency

T will be equal. The dependence of the transmission efficiency T (or reflectivity) on the coupling strength γl with various imperfect internal reflection losses L is plotted as shown in Fig. (3.3). We see that (1) as the coupling strength increases, the transmission efficiency T (or reflectivity R_1, R_2) approaches $1 - L$, restricted only by the reflection loss as expected. Also there always exist certain threshold values which the coupling strength much exceed to achieve appreciable reflectivity. (2) Figure (3.4) shows how the coupling threshold changes as the imperfect internal reflection loss increases. The dependence of the coupling transmission efficiency T and of the phase conjugate reflectivity R_1 on the input beam ratio q with different γl are shown in Figs. (3.5) and (3.6), respectively. These figures give the dynamic range of this kind of device. It is noted that the dynamic range varies substantially when the coupling strength changes.

It was pointed out that competition exists between the self–pumped phase conjugation process[11] and the mutually pumped phase conjugation process.[3,4] This phenomenon may be understood by comparing the coupling strength thresholds for these two different processes. From the two interactive–region theory of the self–pumped phase conjugation,[12] we know that under a lossless situation the threshold of the process is about 4.68. This is lower than the threshold of mutually pumped phase conjugation (BWPC and MIBC) in the symmetric case ($\gamma l_t = 5.0$). This means that the self–pumped phase conjugation process is more favorable than the two–region mutually pumped phase conjugation process for the same coupling strength and loss conditions. In order to achieve the BWPC or MIBC, special care needs to be taken to avoid the self–pumped phase conjugator formation. However, for the asymmetric case, i.e., the coupling strengths of the two regions are different, the threshold of coupling strength changes substantially. For example, when $\gamma_1 l_1 = 6.7$ and $\gamma_2 l_2 = 4.3$, one of which is considerably lower than the threshold of the self–pumped phase conjugator, the mutually pumped phase conjugation process can still be sustained in relatively narrow dynamic range ($0.37 < q < 1.06$). Due to the fact that the coupling thresholds for these various processes are very close, especially

for the MIBC with asymmetric coupling, complicated competition processes might cause bistable behaviors and other interesting phenomena as reported by Eason and Smout.[3,13]

A similar approach is taken to solve the coupled wave equations in order to study the effect of absorption in the one–region DPCM process. The intensities of four beams are obtained in terms of $y(z)$ and Y as:

$$I_1(z) = e^{-\alpha z}\cos^2\left[\frac{y(z) + Y}{2}\right],$$

$$I_2(z) = qe^{\alpha(z-l_1)}\cos^2\left[\frac{y(z)}{2}\right],$$

$$I_3(z) = qe^{\alpha(z-l)}\sin^2\left[\frac{y(z)}{2}\right],$$

$$I_4(z) = e^{-\alpha z}\sin^2\left[\frac{y(z) + Y}{2}\right],$$

(12)

where $y(z)$ and Y are determined by:

$$-2\frac{dy(z)}{dz} = \frac{\gamma}{u_1 + u_2}[(u_1\cos Y + u_2)\sin y(z) + u_1\sin Y\cos y(z)],$$

$$u_1 = e^{-\alpha z},$$

$$u_2 = qe^{\alpha(z-l)},$$

$$y(z)\big|_{z=l} = 0; \quad y(z)\big|_{z=0} = \pi - Y$$

(13)

The coupling transmission efficiency T calculated with various absorptions: ($\alpha = 0$, $\alpha = 2$ cm^{-1} and $a = 4$ cm^{-1}), is shown in Figure (3.7). As expected, when the coupling constant becomes larger and larger, the transmission approaches to $e^{-\alpha l}$. In presence of absorption,

the coupling threshold of DPCM is increased appreciably while the dynamic range of the device decreases substantially. Figure (3.8) shows the intensity distribution inside the photorefractive crystal, from which we can see that pumping beam I_4 is heavily depleted and absorbed at large coupling and absorption and the conjugate beam I_1 builds up monotonically.

Comparison between the performances of the two–region process (BWPC and MIBC) and the one–region process (DPCM) is carried out in Figures (3.9) and (3.10). It is clear that the one–region process has a relatively lower threshold of coupling strength compared with the symmetric two–region process. It also shows higher transmission efficiency or phase conjugate reflectivity. More than 60% transmission has been reported experimentally for the DPCM.[14] The relatively wider dynamic range of DPCM than that of BWPC is evident in Figure (3.10). There is a distinct difference between one–region and two–region processes. In the one–region process the two pumping beams can be different in color. The Bragg condition can be satisfied automatically for the one–region process by angular compensation for the difference in wavelength, as shown in Figure (3.11). However, the Bragg condition can not be satisfied simultaneously in two regions with different wavelengths. That is why no attempt has succeeded to generated BWPC or MIBC without using pump beams of same nominal wavelength.[3,4] Another important feature of the two–region process is that it does not produce spurious conical scattering like DPCM. This often limits the phase conjugate fidelity before its slow collapse. The turn–on time of BWPC), as point out by Ewbank,[4] is noticeably faster than the turn–on time of the DPCM for comparable incident optical powers.

We compare our two–region mutually pumped phase conjugator theory with the experimental results of the BWPC[4] and MIBC.[3] From (10), the ratio of two phase conjugate reflectivities is obtained as

$$\frac{R_1}{R_2} = q^2 \,. \tag{14}$$

The experimental data of BWPC from (5) are fitted with (14), as shown in Figure (3.12), which agrees very well with the theory.

From (5) (6) and the boundary conditions (9), we have the phase conjugate output intensities:

$$I_3(0) = qRcos^2\left[\frac{Y}{2}\right] \, cos^2\left[\frac{Y''}{2}\right] \, e^{-\alpha(d+l_1+l_2)}$$

$$I_1'(l_2) = Rcos^2\left[\frac{Y}{2}\right] \, cos^2\left[\frac{Y''}{2}\right] \, e^{-\alpha(d+l_1+l_2)} \tag{15}$$

and output intensity ratio:

$$\frac{I_3(0)}{I_1'(l_2)} = q \tag{16}$$

The calculated output intensities in the nonabsorption lossless case (i.e., $\alpha = 0$, $L = 0$), where $\gamma_1 l_1 = 6.8$ and $\gamma_2 l_2 = 4.5$, are shown in Figure (3.13), which gives almost the same behaviors as measured values from MIBC in (4). The output intensity ratio of the experimental data is nearly exactly linear, as described by (16).

We introduce a new configuration of mutually pumped phase conjugator: Semilinear Double Phase Conjugate Mirror (SDPCM) and present various experimental studies of the new device.

The basic configuration of the SDPCM is illustrated in Figure (3.14). Two mutually incoherent laser beams are incident on the same side of the photorefractive $BaTiO_3$ crystal. Due to the fanning effect of the material, most of the incident light is fanned asymmetrically along the crystal axis.[15] A spherical mirror placed in both fanning beams images the two incident beams in the crystal onto each other. Two sets of gratings are formed in the separate regions by the interference of each incident beam with its own

fanning beams and the phase conjugate with the feedback fanning beams. The spherical nature of the auxiliary mirror provides a broad angular spectrum of the feedback to allow more gratings to participate in the interaction. Therefore, good phase conjugate fidelity and high reflectivity can be expected in this configuration. As seen in Figure (3.15), two phase conjugate images have been simultaneously achieved with good quality and without any observe cross–talk when two incident beams are spatially modulated by different transparencies. Since the feedback is provided by the controllable external mirror, no competition effect has been observed in the SDPCM between the mutually pumped phase conjugation process and the self pumped phase conjugation process. This is in contrast with the BWPC and MIBC configurations as discussed in previous sections.

The experimental arrangement is shown in Figure (3.16). Linearly polarized light from an Argon ion laser at 514.5 nm passes through a Faraday isolator F, and becomes extraordinarily polarized after rotation by a half wave plate ($\lambda/2$). The incident beam is split into two beams, I_1 and I_2, by a variable beam splitter (VBS). The path difference between beam 1 and 2 is about 30 cm, which is much longer than the coherent length of a multilongitudinal mode Ar^+ laser. The two incident beams are loosely focused to about 1 mm in diameter by a lens L (f = 305 mm) on a single–domain $BaTiO_3$ crystal (5 mm x 5 mm x 5 mm). A spherical mirror of 100 mm focal length and 75 mm in diameter is placed about 10 degrees of the incident beam and images the incident beams in the crystal on each other. The two phase conjugates beams, I_1' and I_2' are monitored with beam splitters BS_1 and BS_2. A Michelson interferometer is formed by BS_2 and M_3 to check if there is a frequency shift of the phase conjugate beam in the SDPCM. The shutter S and three photodetectors are controlled by a computer to study the transient process. PD_1 records the buildup of the phase conjugate beam. PD_2 records the depletion of the incident beam and PD_3 records the evolution of the oscillating fanning beams.

The behavior of the phase conjugate reflectivity as a function of the angle between incident beams and c axis was investigated by rotating the $BaTiO_3$ crystal. The incident

beams were set to be of equal intensity and not necessarily parallel. As shown in Figure (3.17), no phase conjugate beams are generated until the angle reaches about 26 degrees. As the crystal was further rotated, the phase conjugate reflectivities increased rapidly and gradually became saturated. The broad solid angle of the spherical mirror in this configuration provides the freedom for the oscillating fanning beams to choose the optimized coupling directions. More than 20% reflectivity (without taking the Fresnel surface reflection into account) is achieved in the wide acceptance angle as shown in Figure (3.17). It is not difficult to understand the threshold effect of the SDPCM by using the two–interactive region model for mutually pumped phase conjugator as discussed in the previous section. When the coupling strength of the material is below a certain threshold which is determined by the coupling efficiency between two regions, material absorption, and the input beam ratio, etc., self–oscillation in the phase conjugator can not be maintained. From earlier studies[16] of the photorefractive beam coupling experiment, we know that the coupling coefficient is essentially small when the coupling beams are incident at small angles with the optical axis. As the crystal was rotated, the coupling strengths increased and exceeded the threshold of oscillation so that two phase conjugate beams were generated simultaneously. Stable Michelson interference fringes were observed over the whole oscillating angular range, which indicates that there is no frequency shift in the SDPCM. The different mirror coupling efficiencies for the two interactive regions is believed to be the reason for the difference of the two phase conjugate reflectivities.

Next the change of the reflectivities with the incident beam ratio was studies. The incident angle was fixed at 54⁰ with respect to the crystal axis. As shown in Figure (3.18), a large dynamic range and over 250% phase conjugate reflectivity have been observed in this configuration. Two factors are presumably responsible for the large dynamic range of the SDPCM: (a) the long interaction length gives a high photorefractive coupling gain; (b) separation of the two incoherence incident beams reduces the effect of mutual erasure.

No conical scattering ring is observed in the SDPCM configuration. Such

scattering, as discussed before, often limits the phase conjugate fidelity in the DPCM configuration before its slow collapse. However, since the SDPCM is also a two—interactive region device and the phase matching condition can not be satisfied simultaneously in two regions with different wavelengths, it works only with two laser beams of the same nominal wavelength. The experimental studies of the dynamical behaviors of the SDPCM are presented in the next section.

4.   The Study of Transient Processes

Several studies have been conducted on the transient phase conjugation in Kerr media and photorefractive material. Fisher et al.,[17] using the concepts of transfer function and impulse response, studies the transient effect of phase conjugation in Kerr media. Papen et al.,[18] with similar approaches, investigated the standard four—wave mixing geometry in photorefractive material including the relaxation of the material. A strong undepleted pump approximation was applied in both studies. However, due to the highly nonlinear beam coupling and the self—oscillation nature of the mutually pumped phase conjugators, the undepleted pump approximation is not valid in the present study. Time—dependent coupled wave equations have to be solved with specified boundary and initial conditions of various configurations of MPPC. Transient buildup studies have been carried out in the photorefractive two—wave mixing process and the unidirectional ring resonators recently.[19,20] Chaotic behavior has been found in the self—pumped conjugate mirror and "driven" double phase conjugate mirror.[21,22]

In this section we investigate theoretically and experimentally the transient buildup process of a photorefractive double phase conjugate mirror, a one—region process of mutually pumped phase conjugation. A set of four—wave mixing equations coupled with evolution of the space—charge electric field in the material is solved numerically. The buildup time of the DPCM is studied with respect tot he total intensity, the steady—state photorefractive coupling strength, the incident beam ratio, the external electric field and the "seeding" level Experimental measurements of the transient phenomena of a double

phase conjugate mirror (DPCM) and a semilinear double phase conjugate mirror (SDPCM) will be presented.

We consider the interaction of two mutually incoherent waves, A_2 and A_4, incident on the photorefractive crystal, forming the double phase conjugate mirror as shown in Figure (3.2). Two phase conjugate beams, A_1 and A_3, are initiated from the fanning effect of the photorefraction material.[23] The transmission grating, $A_1 A_4^* + A_2^* A_3$ formed by the interference between pumping beams and phase conjugate beams, respectively, is reinforced during the writing and reading process.

Any studies of the transient phase conjugation problem must involve the dynamics of the nonlinear material and the dynamics of the optical fields in a self–consistent manner. The four optical fields are governed by the Maxwell wave equation with the slowly varying envelope approximation (SVEA).[24] The dynamics of the material is obtained by a slight generalization of the Kukhtarev model of photorefractive transient two beam coupling.[25] For four amplitudes A_i (i = 1 ... 4) and E_1, the space–charge electric field E_1 of the material,

$$\left[\frac{\partial}{\partial z'} + \frac{nL}{c\tau_d} \frac{\partial}{\partial t_N} \right] A_1 = j\Gamma L \left[\frac{E_1}{E_Q} \right] A_4, \tag{17a}$$

$$\left[\frac{\partial}{\partial z'} - \frac{nL}{c\tau_d} \frac{\partial}{\partial t_N} \right] A_2 = j\Gamma L \left[\frac{E_1}{E_Q} \right]^* A_3, \tag{17b}$$

$$\left[\frac{\partial}{\partial z'} - \frac{nL}{c\tau_d} \frac{\partial}{\partial t_N} \right] A_3 = j\Gamma L \left[\frac{E_1}{E_Q} \right] A_2, \tag{17c}$$

$$\left[\frac{\partial}{\partial z'} + \frac{nL}{c\tau_d} \frac{\partial}{\partial t_N} \right] A_4 = j\Gamma L \left[\frac{E_1}{E_Q} \right]^* A_1, \tag{17d}$$

$$\frac{\partial}{\partial t_N} \left[\frac{E_1}{E_Q} \right] + A \left[\frac{E_1}{E_Q} \right] = B \frac{A_1 A_4' + A_2' A_3}{I_o}, \tag{17e}$$

where z' is the normalized distance with respect to the crystal L, t_N is the normalized time with respect to the dielectric relaxation time τ_d, i.e., $t_N = t/t_d$. n is the index of refraction of the material. Γ is the coupling constant, which is a function of optical frequency, material parameters and relevant components of the electro–optic tensor. I_0 is the total intensity. According to the theory developed by Heaton and Solymar,[19] the parameters A and B are defined as follows:

$$A = \frac{1}{D}\left[1 + \frac{E_D}{E_Q} + j\frac{E_0}{E_Q}\right],$$

(18a)

$$B = \frac{1}{D}\left[-\frac{E_0}{E_Q} + j\frac{E_D}{E_Q}\right],$$

(18b)

$$D = 1 + \frac{E_D}{E_M} + j\frac{E_0}{E_M}.$$

(18c)

There are four electric fields appearing in Eq. (17) and (18) besides E_1. E_0 is the external dc field applied to the crystal. E_Q, E_M and E_D are material constants defined by:

$$E_Q = \frac{eN_A^-}{K\epsilon_s}, \quad E_M = \frac{\gamma_R N_A^-}{K\mu}, \quad E_D = \frac{KTk_B}{e},$$

(19)

where e is the electron charge, k_B is Boltzmann's constant, T is the absolute temperature, K is the length of the grating vector, μ is the electron mobility, γ_R is the electron recombination time, ϵ_s is the static field dielectric constant, N_A^- is the concentration of ionized accepters. If we neglect the dark current in the material, the dielectric relaxation time τ_d is inversely proportional to the total intensity of light I_0 according to the Kukhtarev model.[26] The absorption of the material is neglected in this treatment.

For general photorefractive materials, the dielectric relaxation time constant τ_d, which governs the speed of index grating formation, is usually on the order of milliseconds to tens of seconds, depending upon the total intensity. The characteristic dimension of a photorefractive crystal is usually less than 1 cm. Thus, we can see that the coefficient of the time derivative terms in Eqs. (17a–d) is so small ($nL/c\tau_d \simeq 10^{-7}$ or less) that the optical waves can be treated as adiabatically following the space–charge field. With the time derivatives dropped from Eqs. (17a–d), we have:

$$\frac{\partial A_1}{\partial z'} = j\Gamma L\left[\frac{E_1}{E_Q}\right] A_4 , \qquad (20a)$$

$$\frac{\partial A_2}{\partial z'} = -j\Gamma L\left[\frac{E_1}{E_Q}\right]^* A_3 , \qquad (20b)$$

$$\frac{\partial A_3}{\partial z'} = -j\Gamma L\left[\frac{E_1}{E_Q}\right] A_2 , \qquad (20c)$$

$$\frac{\partial A_4}{\partial z'} = j\Gamma L\left[\frac{E_1}{E_Q}\right]^* A_1 , \qquad (20d)$$

and the equation for E_1

$$\frac{\partial}{\partial t_N}\left[\frac{E_1}{E_Q}\right] + A\left[\frac{E_1}{E_Q}\right] = B\frac{A_1 A_4^* + A_2^* A_3}{I_0} , \qquad (20e)$$

When we set the temporal derivative in Eq. (20e) equal to zero, i.e., the grating is in steady state, Eq. (20) is reduced to the standard four–wave mixing equation in the transmission grating with the steady–state photorefractive coupling strength γL, where

$$\gamma L = -j\Gamma L\frac{B}{A}. \qquad (21)$$

This has been treated thoroughly by Cronin–Golomb *et al.*[1]

We consider the transient problem by switching on two pumping beams, A_2 and A_4. at the normalized time $t_N = 0$. The boundary conditions for the double phase conjugate mirror can be expressed as follows:

$$A_1(0, t_N) = 0, \quad A_2(1. \, t_N) = A_{20}(constant),$$

$$A_3(1, t_N) = 0, \quad A_4(0, t_N) = A_{40}(constant). \tag{22}$$

The incident beam ratio q is defined as $|A_{20}|^2/|A_{40}|^2$. The space–charge electric field $E_1(z', t_N)$ is assumed to be zero before the pumping beams are turned on, i.e., $E_1(z', 0) = 0$. We assume that there are some uniform "seeds" of light in the direction of A_1 and A_3 *right after* the pumping beams are turned on. They originate by the scattering from A_4 and A_2. Therefore, we have

$$A_1(z', \Delta t_N)|_{z' \neq 0} = \epsilon A_{40}, \quad A_3(z', \Delta t_N)_{z' \neq 1} = \epsilon A_{20} , \tag{23}$$

where ϵ is the seeding coefficient and Δt_N is small.

In finding the solutions of the coupled equations, Eq. (20) and (20e), we use our physical intuition. We assume that for a short enough time interval Δt_N all four beams A_1, A_2, A_3 and A_4 remain unchanged with respect to time but their interference causes the emergence of the space–charge field E_1 at Δt_N. Since, during the interval Δt_N the four beams are independent of time, $E_1(\Delta t_N)$ may be obtained analytically from Eq. (20e)

$$E_1(\Delta t_N) = \frac{B}{A} \left[\frac{A_1(\Delta t_N)A_4^*(\Delta t_N) + A_2^*(\Delta t_N)A_3(\Delta t_N)}{I_0} \right](1 - e^{-A\Delta t_N})E \tag{24}$$

This small space–charge field causes interaction among four waves according to Eqs. (20a–d). Thus, the spatial dependence of four optical waves may be integrated out by standard numerical methods. In return for new interference pattern changes the space–charge field in the next time interval Δt_N. This process continues for further times steps so that we can find optical amplitudes at any position. The criterion of convergence is simply set as the solutions without sensitive dependence of the step sizes.

We mainly study the diffusion–dominated photorefractive effect ($E_0 = 0$) in the double phase conjugate mirror, in which the steady–state coupling strength γL is a real number as seen from Eq. (18) and (21). Eqs. (20a–d) and (20e) are numerically integrated as discussed above with the boundary and initial conditions specified by Eq. (22) and (23) to investigate the following properties:

- (a) The buildup time of DPCM as a function of total intensity I_0.
- (b) The buildup time as the coupling strength γL changes.
- (c) The effect of beam ratio q on the buildup time.
- (d) The effect of "seeding" level or external electric field E_0 on the DPCM response time.

A typical transient buildup of the phase conjugate reflectivity R, defined as $R = I_3(0)/I_{40}$, with the normalized time t_N is shown in Figure (4.1) The *response time* Γ_t of the DPCM is defined as the time of which phase conjugate reflectivity reaches 90% of its steady state value. This definition may be arbitrary simply because the transient process is not an exponential buildup. A reference time is needed to characterize the speed of the DPCM for certain parameters.

First, we study how the buildup time Γ_t responds to the total intensity I_0. We integrate the Eq. (20) and (20e) without changing any parameters as in Figure (4.1) other than *increasing* and *decreasing* the total intensity I_0 by a factor of 10. After plotting the

phase conjugate reflectivity versus their own normalized time, we found that those two new curves are almost unchanged with the curve in Figure (4.1). However, it is noticed that the dielectric relaxation time τ_d is inversely proportional to the total intensity I_0 in the Kukhtarev model. Therefore, normalized time t_N needs to be rescaled to account for the change of total intensity. Then we find that the buildup time for the double phase conjugate mirror is also inversely proportional to the total intensity I_0.

Secondly, we study the variation of response time Γ_t with respect to the steady–state photorefractive coupling strength γL. All parameters for integrating Eq. (20) and (20e) are changed except for varying the effective coupling ΓL expressed in Eq. (21). This is equivalent to changing the effective electro–optic coefficient by rotating the photorefractive crystal.[16] As shown in Figure (4.2) the response time Γ_t quickly decreases as the coupling strength γL increases and tends to saturate at high coupling gain. The phase conjugate beams can never be established when the steady–state coupling strength γL is less than the threshold $\gamma L_t = -2$, which is consistent with the results of the steady–state solutions.[1,2] Figure (4.3) shows the beam ratio q dependence of the response of the DPCM. As q becomes more deviated from unity (equal pumping intensities), the buildup time Γ_t becomes slower while the total intensity I_0 remains unchanged. Finite dynamic range is also observed in the numerical simulations, which is consistent with the previous steady–state studies.[1]

Even though the double phase conjugate mirror is a passive device, seed light is still needed for the induced–oscillation. It may actually come from the scattering of the pumping beams by defects in the crystal. However, the magnitude of the seed light can also affect the response time of the DPCM. We examine this influence by changing the seeding coefficient ϵ within a reasonable range. As the seeding coefficient ϵ becomes larger, i.e., the scattering is stronger, the buildup time Γ_t of DPCM is faster and soon becomes saturated as shown in Figure (4.4). Injection of a strong driving beam along the direction of the beam 1 can cause unstable as well as chaotic output of the phase conjugate beam 3

in this so called "driven" DPCM.[22] However, "driven" DPCM has already lost the meaning of double phase conjugation in the sense of *simultaneously generating two phase conjugate replicas.*

The effect of an external dc field, E_0, applied to DPCM is also numerically studied in this section. Although no external electric field is usually applied to crystals like $BaTiO_3$, SBN, $KNbO_3$ because of their high electro—optic coefficients, other crystals such as BSO, BGO, $GaAs$, etc., often need the external field to enhance the photorefractive coupling gain. We take $BaTiO_3$ as an example where $N_A^- = 10^{16} cm^{-3}$, $\mu\tau_e = 10^{-14} m^2/V$, $\epsilon_s = 150$, $\lambda = 514.5 nm$, $T = 300 K$, $\theta = 5^0$. The interaction length L and the effective coupling coefficient Γ, which is determined by the relevant electro—optic tensor elements and the orientation of optical axis, are chosen such that the steady—state coupling strength γL without external field as: $\gamma L = -3$. The transient buildups of phase conjugate reflectivity are obtained in the case of equal pumping as shown in Figure (4.5). It is clear that the application of an external dc field E_0 has enhanced the phase conjugate reflectivity as well as the speed of DPCM. This is consistent with the experimental study performed by Feinberg et al.[27] in which four—wave mixing gain is enhanced by applied electric field in photorefractive $BaTiO_3$.

The experiment study is performed in the arrangement as shown in Figure (4.6). Linearly polarized light from an Argon ion laser at 514.5 nm passes through a Faraday isolator F, and becomes extraordinarily polarized after the rotation by a half wave plate ($\lambda/2$). The incident beam is split into two beams, A_2 and A_4, by a variable beam splitter VBS. The path difference between the two beams is much longer than the coherent length of a multilongitudinal mode $Ar+$ laser. The two beams are loosely focused to about 1 mm in diameter by lenses, L_1 and L_2 ($f_1 = f_2 = 165$ mm), on a single—domain $BaTiO_3$ crystal (5mm x 5 mm x 5mm), which is on the center of a rotation stage. The angle between A_2 and A_4 is 155^0 while the incident angle of A_2 with respect to the optical axis can be adjusted by rotating the stage. The transients are recorded in a personal computer through

the analog to digital (A/D) interfaced photodetectors, PD_1 and PD_2. PD_1 records the phase conjugate output and PD_2 monitors the evolution of the fanning and conical scattering. A mask is placed in front of the curved mirror M_3 to block the phase conjugate so that only the fanning and conical scattering can be collected in PD_2.

The typical DPCM transient process is shown in Figure (4.7). The fanning beams build up rapidly after the two pumping beams turned on. However, they quickly collapse as the phase conjugate beams emerge. The conical scattering takes longer to collapse as seen from the second slow drop in PD_2. The build up time of DPCM is still defined as the time when phase conjugate beam reaches 90% of its steady–state value. We first measured the response time for different incident intensities. Between each measurement a strong incoherent ordinary light is illuminated on the $BaTiO_3$ crystal for about 5 minutes so that the grating can be totally erased. The input beam ratio is set to be equal and the incident angle of A_2 with respect to crystal axis is 62°. Figure (4.8) shows the response time of DPCM as a function of the incident intensity. The best fit of data yields the expression:

$$t_{DPCM}(sec) = (9.91 \pm 1.03)I^{(0.52\pm0.01)}(W/cm^2) \qquad (25)$$

Secondly, we measure the response time as a function of the incident angle between A_2 and the crystal axis, in which the intensity of two pumping beams is equal to 0.72 W/cm^2 and keeps unchanged during the measurement. Since the increase of the incident angle within certain a range corresponds to approximately linear increase of the steady–state photorefractive coupling strength[16], we put the experimental data with the theoretical curve in Figure (4.2), which shows a good qualitative agreement between theory and experiment. The transient behavior may be somewhat oscillatory or quite complicated if the beams are not properly overlapped. Further study is needed to characterize the cause of these instabilities.

The dynamical process of the Semilinear Double Phase Conjugate Mirror (SDPCM)

is also investigated experimentally in the arrangement shown in Figure (3.16). The transients ares recorded in a personal computer through the A/D interface photodetectors, PD_1, PD_2 and PD_3. PD_1 records the build up of the phase conjugate beam. PD_2 monitors the transmitted beam while PD_3 records the solution of the oscillating fanning beams. The typical transient process of the SDPCM is shown in Figure (4.9), which is recorded with total intensity of 1.53 W/cm^2, beam ratio $q = 1$, and incident angles at 54 degrees. The transmitted beam begins to be depleted right after the shutter is opened. Since the fanning beam always plays an important role in the passive phase conjugation devices, it is carefully monitored by the photodetector PD_3 from the reflection by the crystal surface. As seen in Figure (4.9), the fanning beams build up immediately until the phase conjugate beam begins to rise. The apparent slow down of the fanning build up indicates that the phase conjugation process gradually dominates the spontaneous fanning process of the photorefractive material and the fanning is becoming a part of the oscillating beam of the phase conjugator. Figure (4.10) shows the different transient behavior of the oscillating fanning in the SDPCM and the spontaneous fanning of $BaTiO_3$, which is recorded by slightly tilting the feedback beams of the spherical mirror outside the range for the phase conjugation. The response time of the SDPCM is significantly faster than the self–pumped phase conjugate mirror (or cat mirror),[15] as compared in Figure (4.11), for the same total intensity of 1.53 W/cm^2. Considerable difference of the build up time of the SDPCM is observed ranging from a few seconds at large incident angles to tens of minutes at small incident angles. This is qualitatively consistent with the theoretical studies of the one–region mutually pumped phase conjugator.

In the section we have numerically solved the coupled nonlinear equations and studied how the build up time is dependent on various parameters. Experiments have been performed to verify these effects. In comparison of the theoretical and experimental results we find that a discrepancy arises in the study of the response time as a function of total intensity. In the theoretical analysis the response time of DPCM is found to be inversely

proportional to the total intensity, which is reasonable and consistent with the Kukhtarev model of photorefractive effect. However, the experimental studies yield the sublinear dependence as shown in Eq. (4.9). Two factors are believed contributing to the discrepancy. First, the build up of the phase conjugate beam from DPCM is nearly equivalent to the formation of refractive—index grating. The discrepancy between theory and experiment on the rate of refractive—index grating change to the incident intensity is still unresolved.[28] Various models haves been suggested to resolve this problem.[29] Secondly, we did not include the interactions of the fanning grating into the theoretical model. The more complete picture on the transient process of DPCM is that the fanning gratings build up when pumping beams are turned on. Since only the phase conjugate grating is phase—matched, therefore reinforced during reading and writing processes, other fanning holograms are eventually erased. These processes may be included in future theoretical work to account for the discrepancy.

5.   Novel Applications of MPPC

Since the discovery of the mutually pumped phase conjugation, various applications have been proposed and demonstrated. Due to the unique characteristics of MPPC it has been applied to optical image processing,[30] optical communication,[31,32] beam steering,[14] laser locking,[33] dynamic interconnects,[34,35] optical thresholding,[30,36] interferometry and optical neural networks,[37] etc. No attempt has been made here to cover all the possible applications of MPPC.

In this section we present the experimental studies of MPPC as two—way phase conjugate communication link and investigate the mutually incoherent phase conjugation combined with coherent amplification for communication purposes.

The capability of correcting wavefront distortion by optical phase conjugation was been realized about one decade ago.[24] It provides the potential for applications in atmospheric communication. However, most of the methods for generating phase conjugate

wavefront either require very high optical intensity, which may cause other unwanted nonlinear phenomena, or require mutual coherence between the signal and the pump beams, making them inapplicable for such applications as long distance optical communication.

Mutually pumped phase conjugator in photorefractive materials can simultaneously generate two phase conjugate wavefronts with c.w. mutually incoherent beams. Therefore, it may lead to high efficiency atmospheric optical communication. First we study the temporal modulation behaviors of MPPC. The schematic diagram is illustrated in Figure (5.1). A potential distant receiver A emits a beam beam 1 to open a communication channel with station B. The local source sends a signal beam 3 to interact with the received beam 1 in the photorefractive material, forming a mutually pumped phase conjugator. Beam 2, carrying the temporal information from station B and the distorted spatial wavefront of beam 1, will undo the distortion along the way and reach the station A undistorted. As shown in Figure (5.2), the signal sent from station B (upper trace) is received at station A without observable distortion (lower trace). Station A can not only receive signals from station B but also send information to station B simultaneously. The wavefront detected by D_2 at station B, which is carrying the temporal information from A, is also spatially undistorted even though the signal is coming from the distant source. This is because the local wavefront of beam 3 does not experience any distortion and beam 4 is the phase conjugate of beam 3. Figure (5.3) shows the two received signals at station A and B, respectively, when the two stations are simultaneously sending information with different modulations. No cross-talk is observed in the experiment, which means the MPPC is an inherent two-way communication link without using any division multiplexing techniques. The modulation at each station may be carried out with amplitude, frequency and phase modulation methods as long as the modulation frequency is higher than the photorefractive material time response which is about a few hertz for practical c.w. intensity range. For fast modulation, the upper limit is actually bounded by

the response of detectors and electronics. Of course, the frequency of the signal beams may be broadened and changed by the fast modulations. However, double phase conjugate mirror configuration can be operated with different wavelengths. There may be a theoretical upper modulation limit for the two–interactive region configurations of MPPC such as: BWPC, MIBC, SDPCM, etc., since the phase matching condition can be be simultaneously satisfied at two interactive regions for different wavelengths. We estimate the upper limit by using the theory of volume holography. For volume hologram the diffraction efficiency drops to zero when the wavelength change causes the deviation from the Bragg condition as the following:[11]

$$\frac{\Delta\lambda}{\lambda} = \frac{\sqrt{3}}{2} \frac{\Lambda}{d\tan\theta},$$ (26)

where $\Lambda = 2\pi/K$ is the period of the grating, d is the interaction length, θ is the incident angle for the unslanted volume grating. Roughly, for $\Lambda = 1\mu m$, $d = 1$ mm, $\lambda = 514.5$ nm,

$$\left|\frac{\Delta\nu}{\nu}\right| = \left|\frac{\Delta\lambda}{\lambda}\right| \approx 10^{-3}$$

therefore, $\Delta\nu \approx 100$ GHz. which is much higher than the bandwidth of current modulation device. As long as the modulation rate is higher than the response time of photorefractive material, MPPC does not introduce any distortion to the transmitted signals. Another interesting experiment is performed on the temporal modulation in MPPC. We modulate the two incident beam's amplitude with same frequency but opposite phase so that these two pumping beams are in fact not present in the crystal at the same time. Figure (5.4) shows these two received signals at each station, which means MPPC works as well as in other modulations. This is due to the property of the long erasure time of photorefractive material, two pumping beams do not need to write the same grating within the erasure period.

The signal beam 1 received at station B may be attenuated during the transmission by scattering and absorption. In order to make MPPC work efficiently, local pumping beam 2 has to be about the same intensity level as beam 1. When the phase conjugate beam 4 reaches to D_1 of station A, it could be very weak. To avoid such a problem, the amplification via two—wave mixing scheme is introduced.[36] The basic configuration is schematically shown in Figure (5.5). The weak beacon beam 1 originating at the potential received station A is transmitted through a distorting medium and detected at station B. At station B the distorted beacon beam 1 is directly transmitted through the photorefractive crystal PR_1 and is incident on the photorefractive crystal PR_2. The mutually pumped phase conjugation in PR_2 is spatially phase conjugate of beam 1 but is coherent with beam 5 which carries most of the power from the local laser L_2. Thus, beam 5 may be directed into PR_1 to serve as a coherent pump to amplify beam 4 and generate a strong beam 6 which is also a phase conjugate of beam 1. If beam 5 is temporally modulated, the modulation will be transferred to beam 6 and transmitted toward the distant receiving station A. It is interesting to note that the temporal modulation can be transmitted to beam 6 if either beam 5 is modulated[40] or beam 2 is modulated[41] or both as indicated in Figure (5.5).

The process taking place in crystal PR_1 may be described as a combination of two—beam coupling and four—wave mixing with some contribution from the double phase conjugation effect. Although the latter is weak due to a large intensity difference among the three beams incident on the crystal, there is still an appreciable competition among these processes. In any case, beam 4 is substantially amplified by the strong pump beam 5 producing beam 6 which is temporally modulated with the signal to be transmitted. The amplification process does not change the transversal phase distribution of beam 4, which means beam 6 is also the phase conjugate of the beacon beam 1. Thus, the temporal information originating from laser L_2 is carried by the strong signal beam 6 transmitted back to the source station A, spatially undistorted.

For experimental convenience the distant laser L_1 is replaced by a small fraction of the beam from the local laser L_2 with a very long path difference, which is much longer than the coherent length of the multi–longitudinal mode argon laser used in this experiment. The actual experiment is performed with the configuration depicted in Figure (5.6). We use a total output power of about 80 mW, 60% of which is directed into the pump beam 5 and about 3% transmitted through the beam splitter BS_2. Beam 1', finally reaching the second photorefractive crystal PR_2, is about 0.2 mW, having the Bird–Wing Phase Conjugator formed with beam 2. A substantial part of the apparent power loss in PR_1 is due to a four–wave mixing process to be discussed below, while the rest comes from fanning, Fresnel reflection and absorption which may be reduced by proper coating and improved crystals.

Placing a distorting medium in beam 1 produces after one transit the wavefront as shown in Figure (5.7a). The well–defined spot of Figure (5.7b) shows the wavefront correction attained for the amplified phase conjugated beam 6 after a single transit through the distorting region. The intensity of beam 6 is 500 times stronger than the phase–conjugated beam without amplification (with beam 5 blocked), thus a gain of 500 is achieved. Unfortunately, the combined losses due to Fresnel reflection, absorption and scattering reduced the over all efficiency by a significant factor. Therefore, the absolute power in the return beam 6 is only a factor of 10 larger than the incoming beam 1. In stationary conditions, about 50% of the power in beam 1 is coupled into a beam that is the phase conjugate of beam 5, indicated the presence of an efficient four–wave mixing process alongside the desired two–beam coupling process. The coexistence of these various processes may limit the achievable gain of the whole system. Thus, an attempt to eliminate the four–wave mixing process by polarization manipulation,for example, by using cubit photorefractive crystals,[42] may improve the performance.

Temporal modulation is investigated by placing an acousto–optic modulator operating at 500 kHz in beam 5 and observing beam 6 with the help of an additional beam

splitter. The upper trace of Figure (5.8) is the temporal modulation of beam 5, while the lower trace shows the signal detected from the amplified and phase—conjugated beam 6. The modulation of the amplified beam exactly reproduces the signal modulation except for a small kink visible on the trace. Before discussing the small artifact in the amplified signal in Figure (5.8) we show in Figure (5.9) two similar traces with acousto—optic modulator replaced by a mechanical chopper. Although the modulation frequency is much lower, the signal is slightly distorted to an extent that endangers causality. The puzzle is resolved by recording the intensity over the beam edge separately, as shown in Figure (5.10), where we can see the amplification of the diffraction pattern from the edges of the chopper blades. The combined result is a slight widening at the bottom of the light pulses as seen in Figure (5.9). The small kink in Figure (5.8) has a similar origin; it is due to light scattered from zero—order beam to AO cell, part of which is amplified and transmitted to the detector where it can be observed at the far edges of the main beam as a small signal exactly out of phase with the main beam. There are two important reasons for a closer investigation of the above artifacts: First, they demonstrate a very wide dynamic range, which is combined with a high nonlinearity; second, they indicate what kind of precautions must be taken when performing experiments involving nonlinear effects.

Mutually pumped phase conjugator can be applied to coherent communication. Coherent communication is based on the superposition of an incoming signal beam and a beam from a local oscillator, both having constant transversal phase distribution. This superposition is impossible whenever the wavefront of the incoming beam is spatially distorted and, in particular, if it has a transversely random phase distribution. Since all wavefronts propagating through a real atmosphere are distorted, atmospheric coherent communication is only possible by spatially filtering a very small fraction of the signal beam leading to undetectable power levels, which may also temporarily fade.[43]

To overcome the problems of wavefront matching for coherent communication, mutually pumped phase conjugation may be applied directly since the main characteristic

of MPPC is the wavefront conversion. What remains to be done is mixing the wavefront—corrected signal with the local oscillator beam. A possible heterodyne detector configuration is schematically shown in Figure (5.11): The signal beam from a distant laser L_1 is mixed with a small fraction of the local oscillator beam 2 in the photorefractive crystal PR generating the mutually pumped phase conjugation. As a result, beam 3 is produced with the spatial wavefront of local beam 2 and the temporal modulation of the signal beam 1. Mixing this beam with the major part of the local oscillator beam in beam splitter BS_2 facilitates the heterodyne signal detection in detector D. In practice, a large light—collecting optical system in front of the crystal may be used to enhance the received energy without distorting the beam that is actually heterodyned. The property of the coherent communication system is experimentally investigated by deriving the local oscillator beam from the transmitting laser and observing the interference between the phase—conjugated beam and a direct beam. The distorted interference fringes observed in Figure (5.12a) are obtained without correction while a single fringe over the whole beam is observed in Figure (5.12b) after the wavefront conversion, i.e., mutually pumped phase conjugation.

To conclude this section, it is worthwhile pointing out that we have demonstrated the possibility of improved optical communication through distorting media using photorefractive mutually pumped phase conjugation. Unfortunately, no material is yet available that is capable of allowing the rate of atmospheric fluctuations with reasonable incident beam powers. As material development progresses, the technique demonstrated in this dissertation may lead to highly efficient atmospheric optical communication.

1. M. Cronin–Golomb, B. Fisher, J. O. White and A. Yariv, IEEE J. Quantum Electron. EQ–20, 12 (1984).

2. S. Weiss, S. Sterenklar and B. Fisher, Opt. Lett. 12, 114 (1987).

3. A. M. Smout and R. W. Eason, Opt. Lett. 12, 498 (1987).

4. M. D. Ewbank, Opt. Lett. 13, 47 (1988).

5. Q. C. He, IEEE J. Quantum Electron. EQ–24, 2507 (1988).

6. A. Yariv and S.–K. Kwong, Opt. Lett. 10, 454 (1985).

7. Q. C. He and J. G. Duthie, to be published, Optics Communications.

8. M. Cronin–Golomb, B. Fisher, J. O. White and A. Yariv, Appl. Phys. Lett. 42, 919 (1983).

9. M. R. Belić and M. Lax, Opt. Comm. 56, 197 (1985).

10. M. R. Belić, Phys. Rev. A31, 3169 (19895).

11. J. Feinberg, Opt. Lett. 7, 486 (1982).

12. K. R. MacDonald and J. Feinberg, J. Opt. Soc. Am. 73, 548 (1983).

13. R. W. Eason and A. M. Smout, Opt. Lett. 12, 51 (1987).

14. B. Fisher and S. Sternklar, Appl. Phys. Lett. 51, 74 (1987).

15. M. Cronin–Golomb and A. Yariv, J. Appl. Phys. 57, 49066 (1985).

16. Y. Fainman, E. Klancnik and S. H. Lee, Opt. Eng. 25, 288 (1986).

17. R. A. Fisher, B. R. Suydam and B. J. Feldman, Phys. Rev. A23, 3071 (1981).

18. G. C. Papen, B. A. Saleh and J. A. Tataronis, J. Opt. Am. B5, 1763 (1988).

19. J. M. Heaton and L. Solymar, IEEE J. Quantum Electron. QE–24, 558 (1988).

20. G.Pauliat, M. Ingold and P. Gunter, IEEE J. Quantum Electron. QE–25, 201 (1989).

21. D. J. Gauthier, P. Narum and R. W. Boyd, Phys. Rev. Lett. 58, 1640 (1987).

22. W. Krolikowski, K. D. Shaw, M. Cronin–Golomb and A Bledowski, QELS'89, Baltimore, MD, WDD11 (1989).

23. V. V. Vornov, I. R. Dorosh, Yu. S. Kuz'minov and N. V. Tkachenko, Sov. J. Quantum Electron. 10, 1346 (1980).

24. R. A. Fisher, ed., *Optical Phase Conjugation* (Academic, New York, 1983).

25. N. V. Kukhtarev, V. B. Markov and S. G. Odulov, Opt. Commun. 23, 338 (1977).

26. N. V. Kukhtarev, V. B. Markov, S. G. Odulov, M. S. Soskin and V. L. Vinetskii, Ferroelectrics, 22, 961 (1979).

27. J. Feinberg, D. Heiman, A. R. Tanguay and R. W. Hellwarth, J. Appl. Phys., 51, 1297 (1980).

28. S. Ducharme and J. Feinberg, J. Appl. Phys., 56, 839 (1984).

29. D. Mahgerefteh and J. Feinberg, Opt. Lett., 13, 1111 (1988).

30. S. Sternklar, S. Weiss and B. Fisher, Opt. Eng. 26, 423 (1987).

31. Q. C. He, J. G. Duthie, J. Shamir and H. J. Caulfield, Tech. Digest, Topical Meeting on Photorefraction Materials, Effects and Devices (1987).

32. Q. C. He, J. Shamir and J. G. Duthie, Appl. Opt. 28, 306, (1989).

33. S. Sternklar, S. Weiss, M. Segev and B. Fisher, Opt. Lett 11, 528 (1986).

34. H. J. Caulfield, J. Shamir and Q. C. He, Appl. Opt. 26, 2291 (1987).

35. S. Weiss, M. Segev,, S. Sternklar and B. Fisher, Appl. Opt. 27, 2291 (1987).

36. Q. C. He, J. G. Duthie and D. A. Gregory, Opt. Lett. 14, 575 (1989).

37. G. Dunning, Y. Owechko, B. H. Soffer, Tech. Digest, Optical Society of America 1989 Annual Meeting, WU3 (1989).

38. L. Solymeer and D. J. Cooke, *Volume Holography and Volume Gratings*, (Academic, New York, 1981).

39. J. Shamir, H. J. Caulfield and B. M. Hendrickson, Appl. Opt. 27, 2912 (1988).

40. G. LeSaux, G. Roosen and A. Brun, Opt. Commun. 58, 238 (1986).

41. G. H. deMontchenault, B. Loiseaux and J. P. Huignard, Appl. Phys. Lett. 50, 1794 (1987).

42. P. Yeh, J. Opt. Soc. Am. B4, 1382 (1987).

43. J. Shamir, H. J. Caulfield, M. Ross and B. M. Hendrickson, Appl. Opt. 27, 1389 (1988).

Figure 3.1 — Bird–wing phase conjugator (BWPC)

36
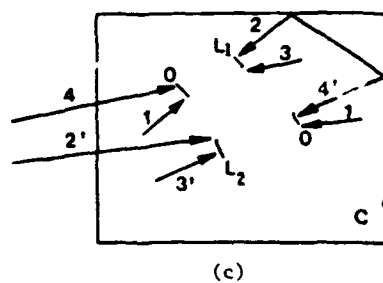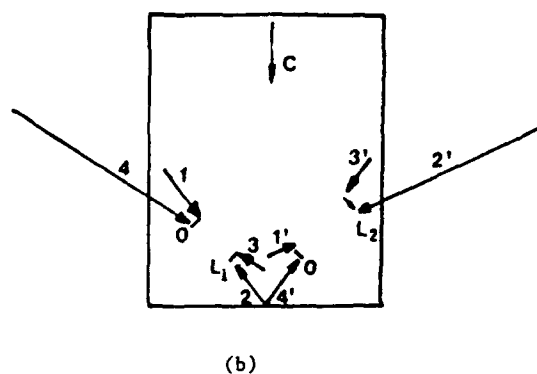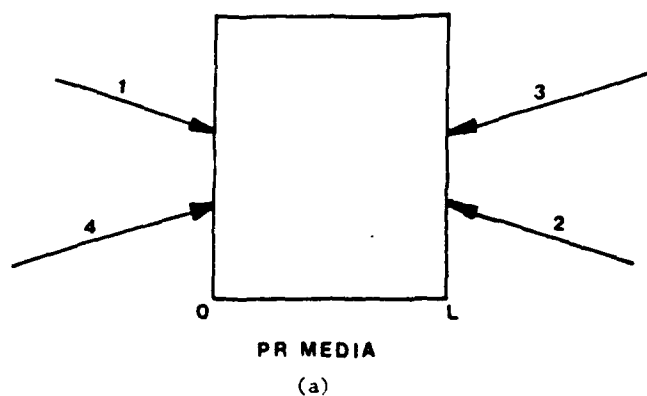
Figure 3.2 — Schematic diagrams of four—wave mixing in mutually pumped phase
conjugators
(a) Double phase conjugate mirror
(b) Bird—wing phase conjugator
(c) Mutually incoherent beam coupler.
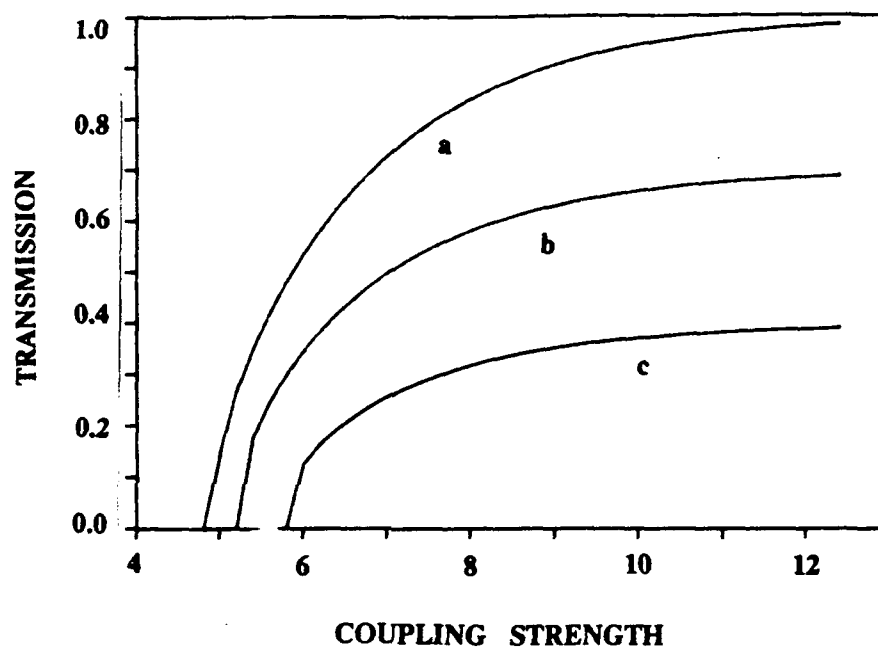
Figure 3.3 — Dependence of the transmission T (or phase conjugate reflectivity) on the coupling strength γl with imperfect internal reflection loss L.
(a) $L = 0$
(b) $L = 30\%$
(c) $L = 60\%$, where $\alpha = 0$, $\gamma_1 l_1 = \gamma_2 l_2 = \gamma l$, q = 1.

38
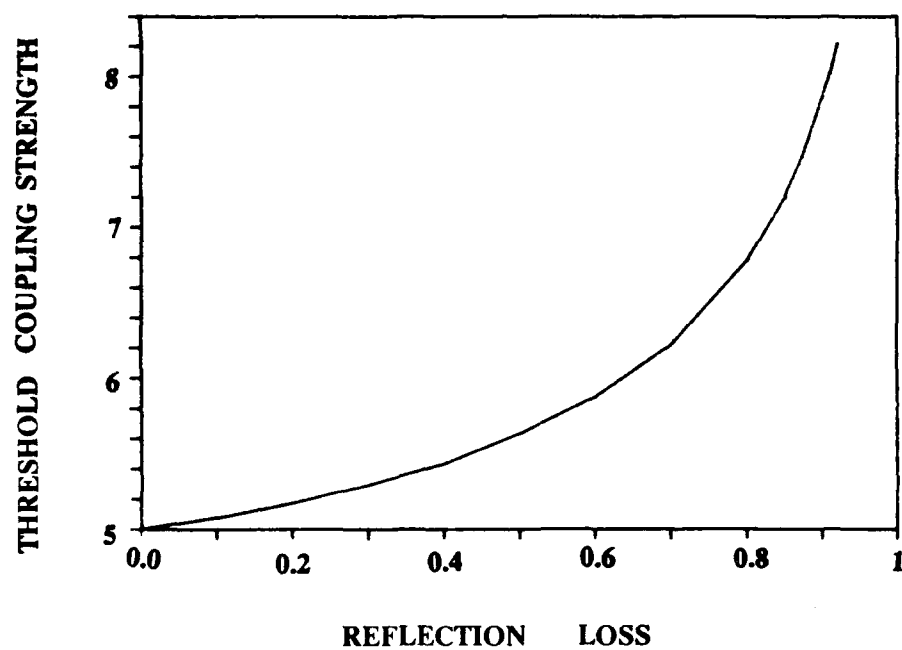
Figure 3.4 — Threshold coupling strength versus imperfect reflection loss L for the symmetric case, i.e., $\gamma_1 l_1 = \gamma_2 l_2 = \gamma l$, q = 1.
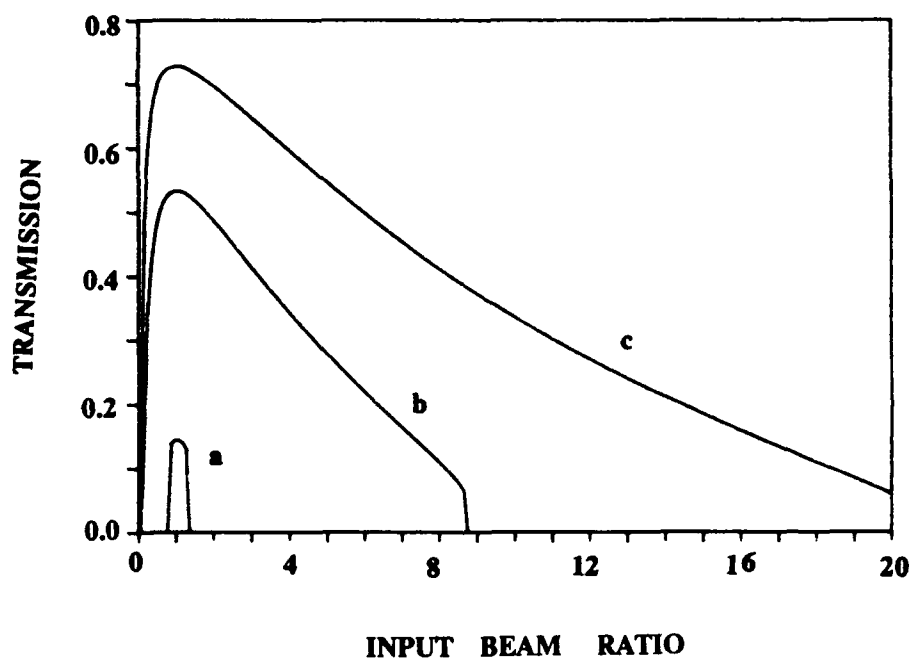
Figure 3.5 — Coupling transmission efficiency T versus input beam ratio q with different coupling strengths.
(a) $\gamma l = 5$
(b) $\gamma l = 6$
(c) $\gamma l = 7$, where $\alpha = 0$, $L = 0$

40
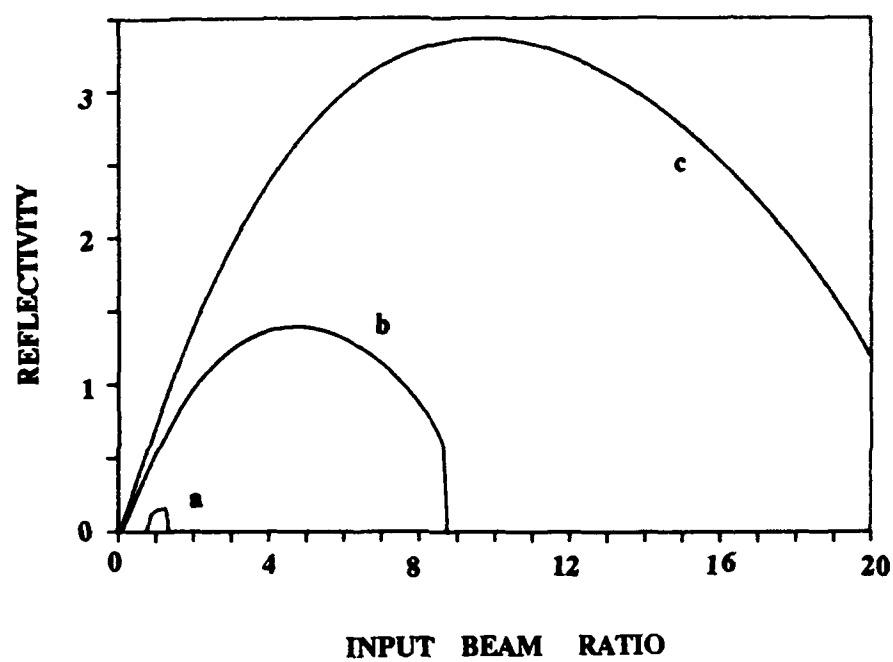
Figure 3.6 — Phase conjugate reflectivity R_1 versus input beam ratio q with different coupling strengths.
(a) $\gamma l = 5$
(b) $\gamma l = 6$
(c) $\gamma l = 7$, where $\alpha = 0$, $L = 0$
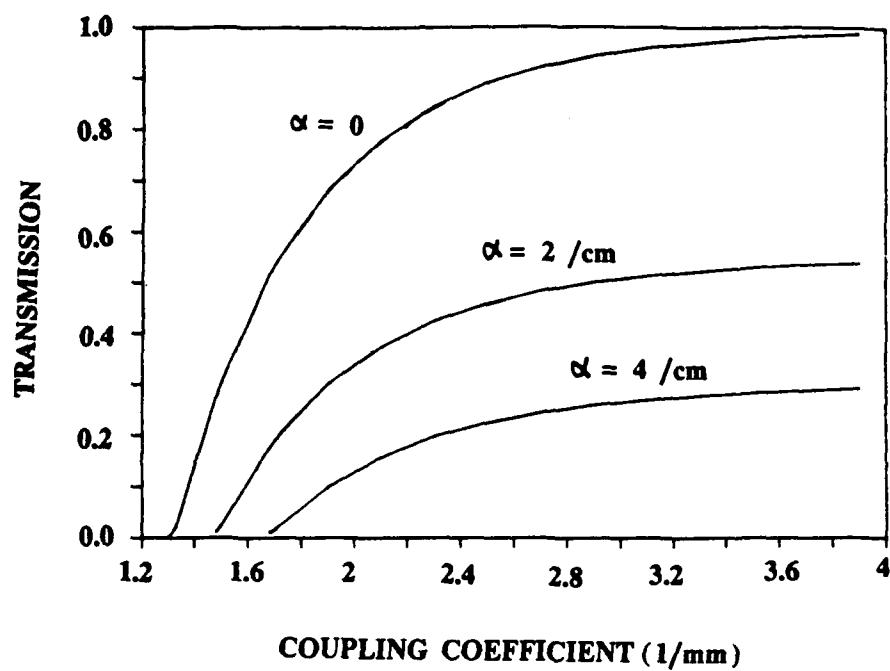
Figure 3.7 — Coupling transmission efficiency T versus coupling coefficient γ with different absorptions, where $l = 3mm$, $q = 1$.
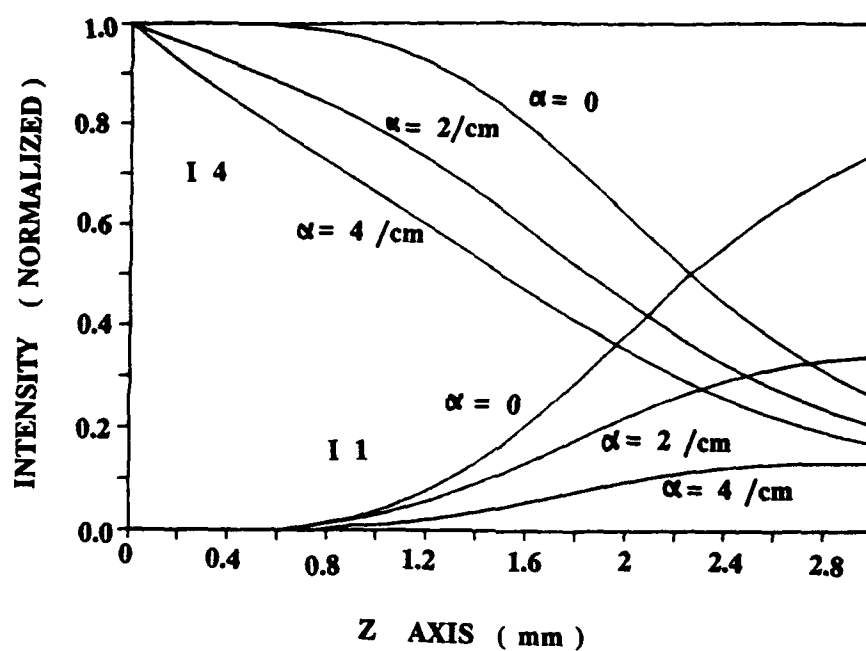
Figure 3.8 — Intensity distribution of I_1 and I_4 inside the crystal with different absorptions, where $\gamma = 2mm^{-1}$, $q = 1$.
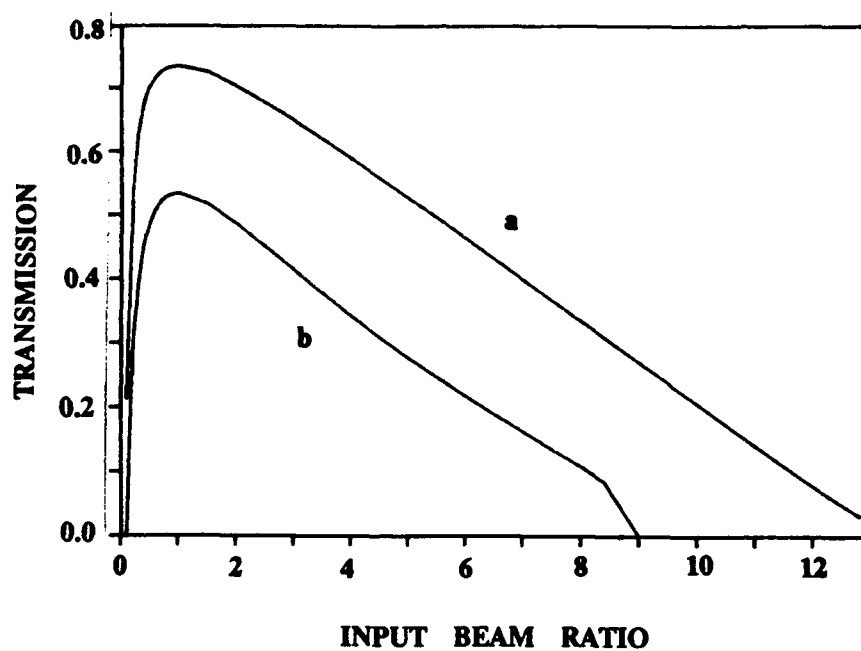
Figure 3.9 — Comparison of one–region process and two–region process of MPPC in the lossless symmetric case, i.e., $\alpha = 0$, $L = 0$, $q = 1$. Transmission versus coupling strength.
(a) One–region process
(b) Two–region process
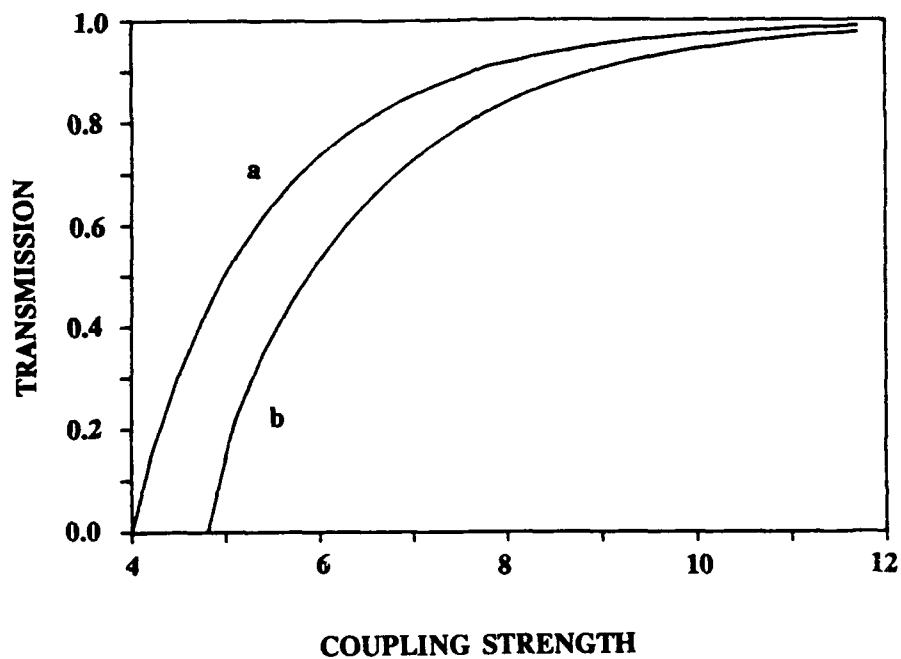
Figure 3.10 — Comparison of one—region process and two—region process of MPPC in the lossless case, i.e., $\alpha = 0$, $L = 0$, $q = 1$. Coupling transmission versus input beam ratio.
(a) One—region process
(b) Two—region process
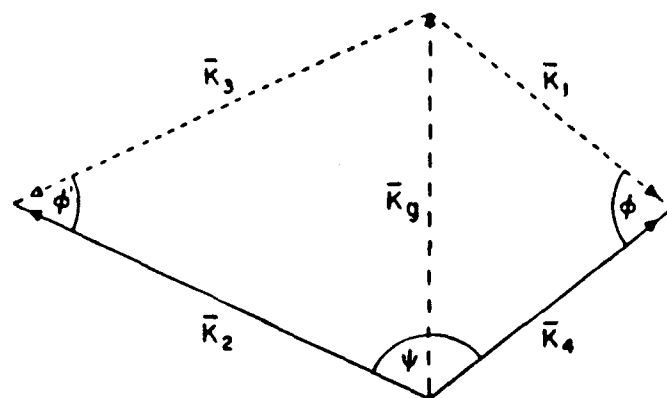
Figure 3.11 — Phase matching diagram of $\vec{k}$ vectors and gratings. $|k_1| = |k_4| = 2\pi/\lambda_1$ and $|k_2| = |k_3| = 2\pi/\lambda_2$ (after Fisher, et al.).
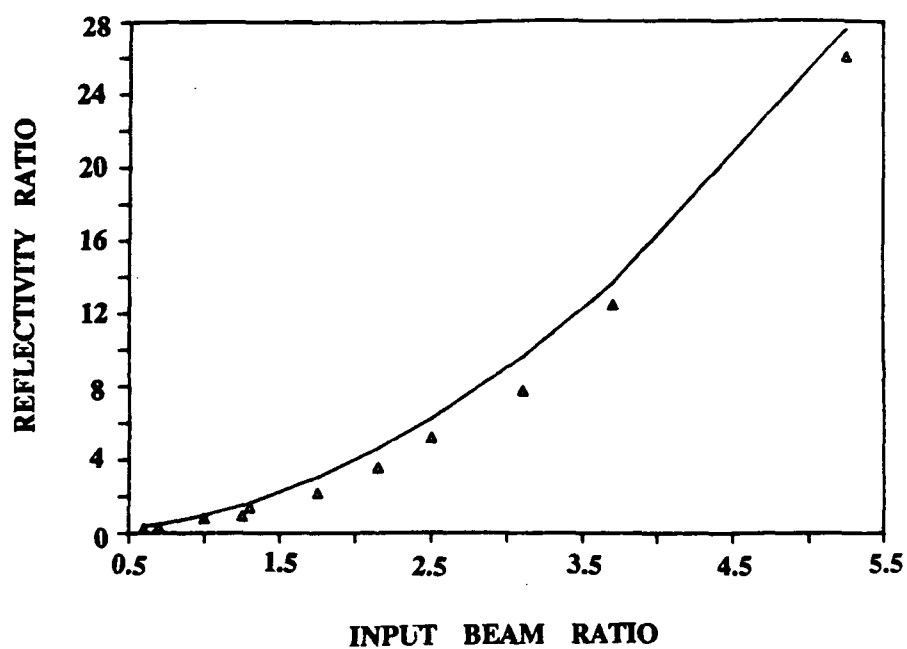
Figure 3.12 — Phase conjugate reflectivity ration R_1/R_2 of the two—region process versus the input beam ratio q. The solid line is the theoretical result and the triangles are experimental data of BWPC where lateral beam position $x = 3.5mm$.
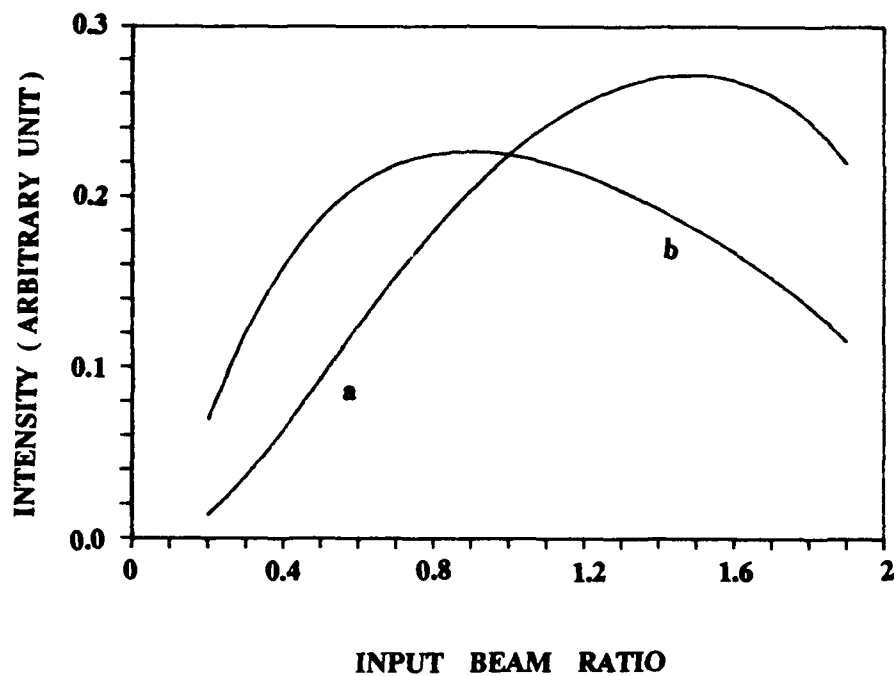
Figure 3.13 — Phase conjugate intensities of the two–region process (MIBC) versus the input beam ratio q in a lossless case $L = 0$, where $\gamma_1 l_1 = 6.7$; $\gamma_2 l_2 = 4.5$.
(a) Intensity I_3
(b) Intensity I_1 (I_2)
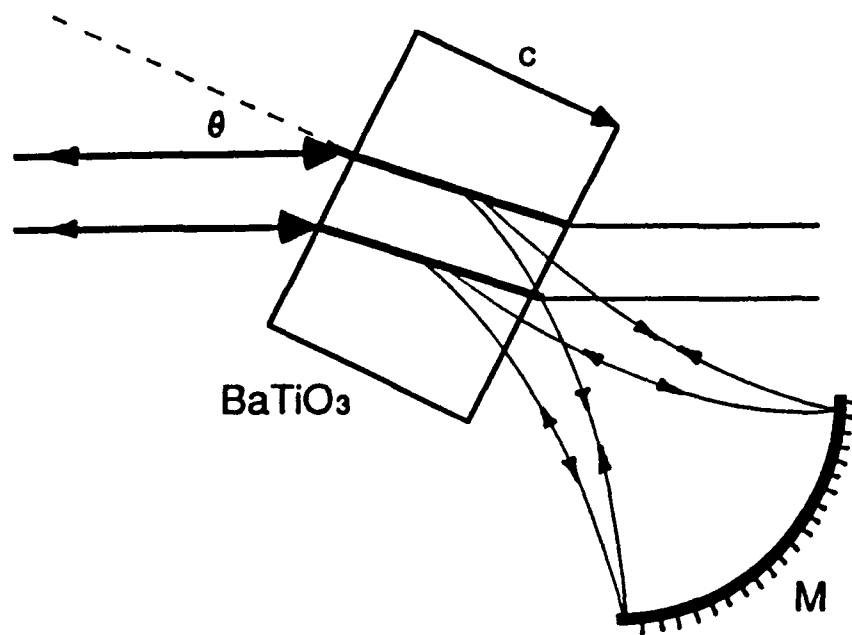
Figure 3.14 — Schematic diagram of the semilinear double phase conjugate mirror (SDPCM). M, spherical mirror.

Figure 3.15 — Phase conjugate images simultaneously generated by the SDPCM.
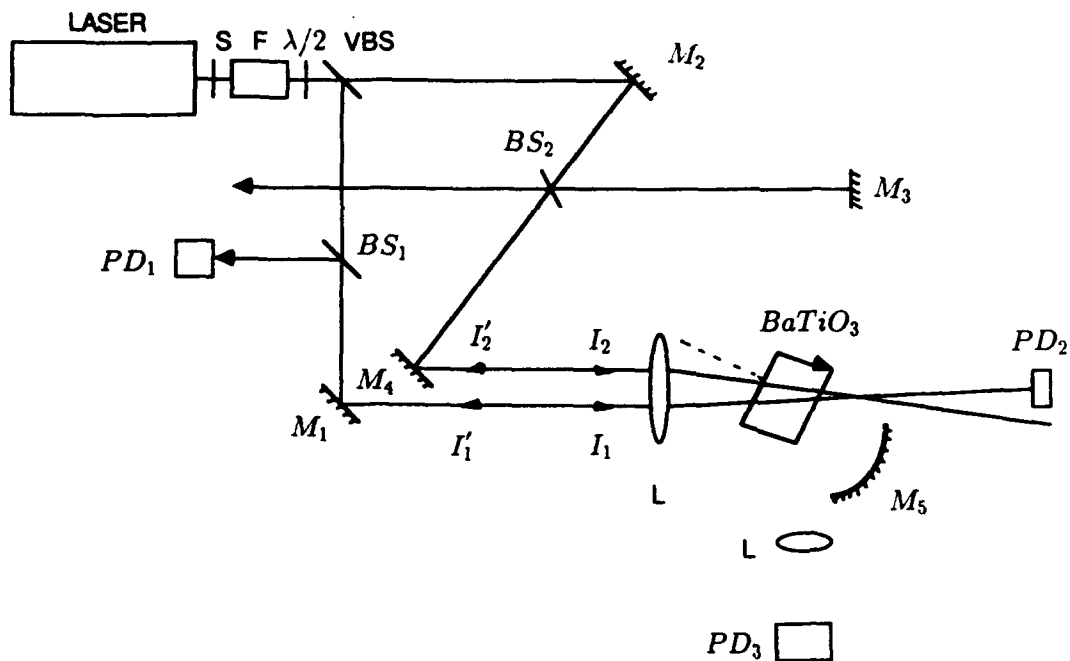
Figure 3.16 — Diagram of experimental apparatus. F, Faraday isolator; $\lambda/2$, half–wave plate; VBS, variable beam splitter; PD's, photodetectors; Ml'ks, mirrors; BS's, beam splitters.
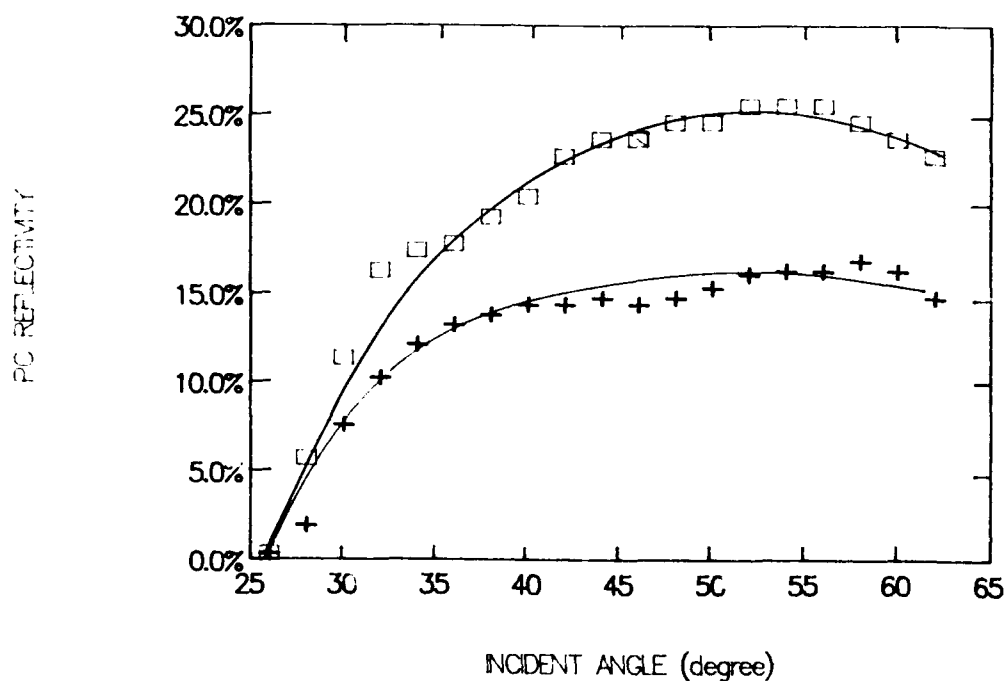
Figure 3.17 — Experimental measurement of the phase conjugate reflectivities (without correction of Fresnel losses) vs. the incident angle as indicated in Figure 3.14 with the beam ratio being unity. R_1 and R_2 are defined as I_1'/I_1 and I_2'/I_2, respectively.
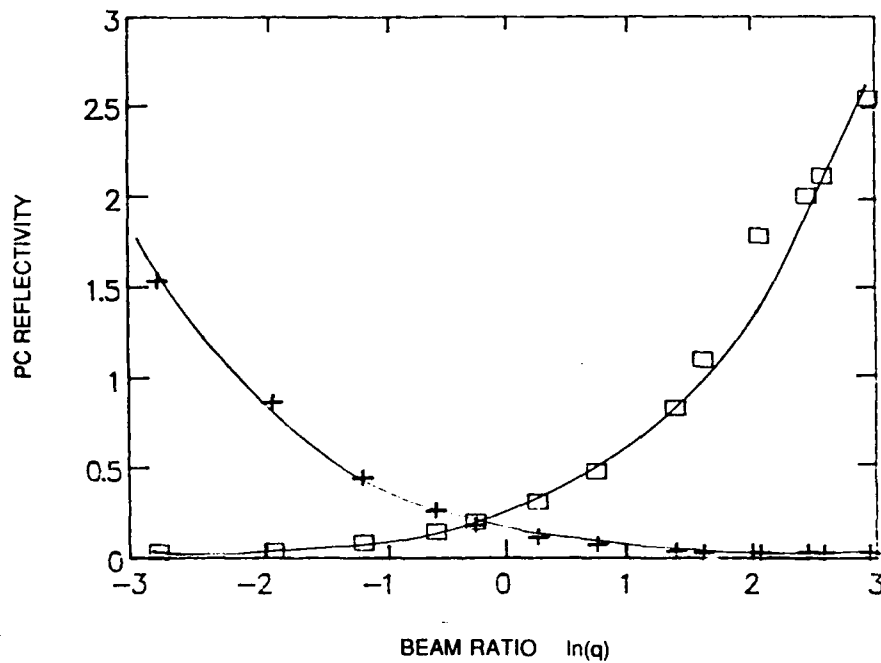
Figure 3.18 — Experimental measurement of the phase conjugate reflectivities (without correction of Fresnel losses) vs. the incident beam ratio q ($q = I_2/I_1$) with incident angle at 54°.
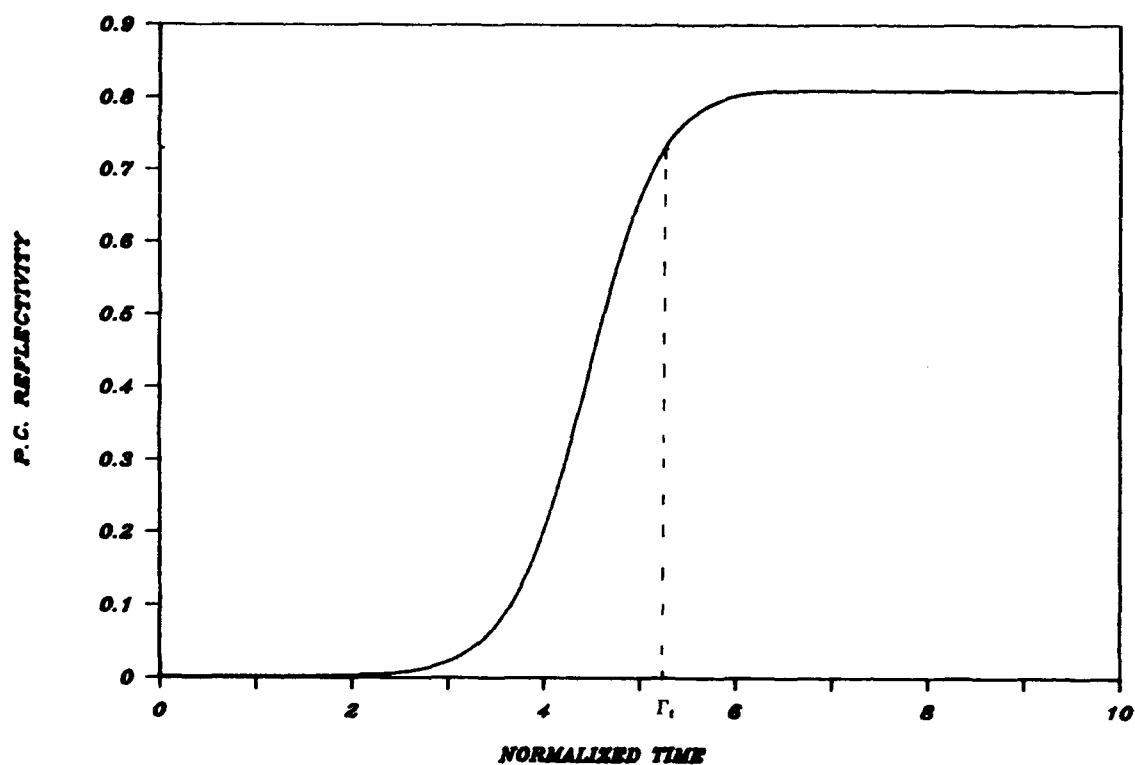
Figure 4.1 — Typical transient build up of the phase conjugate reflectivity R, defined as $I_3(0)/I_{40}$ of DPCM, with $I_0 = 1$, $q = 1$, $A = (1, 0)$, $B = (0, 2)$, $\Gamma L = -6$.
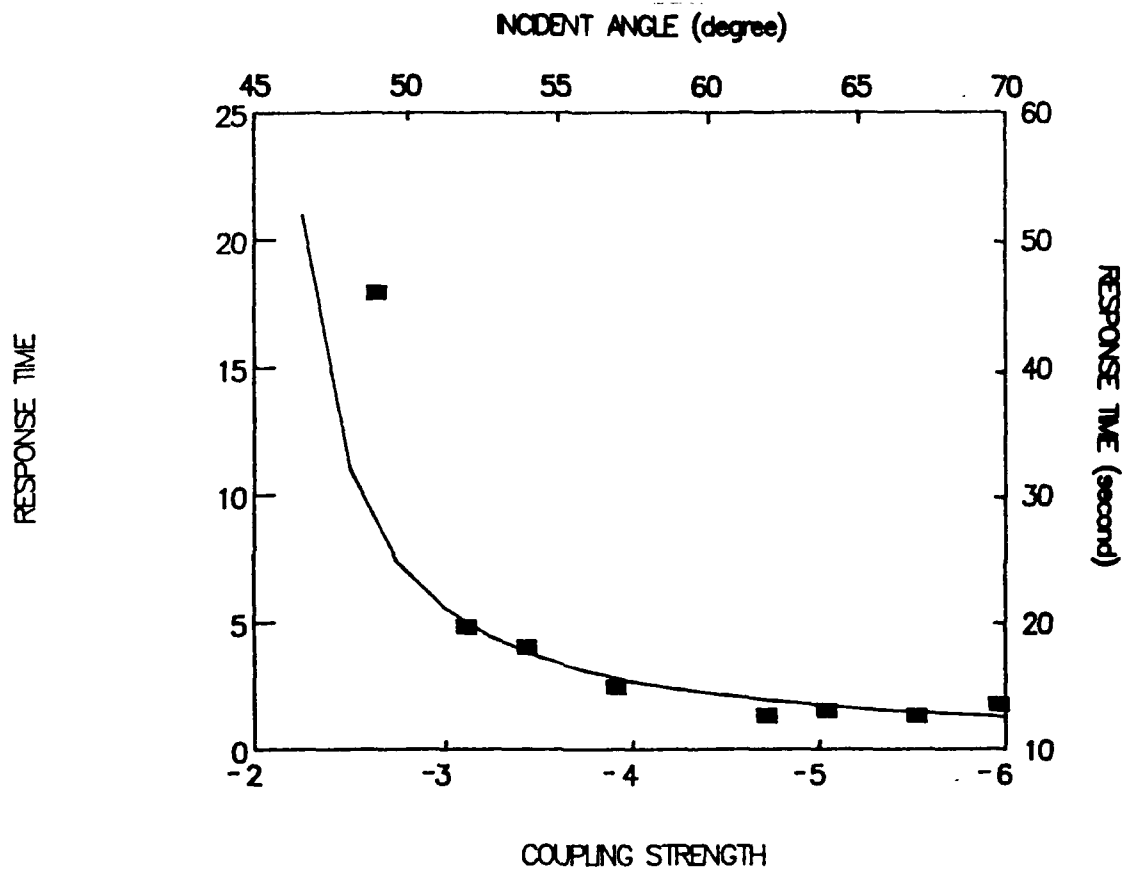
Figure 4.2 — Response time Γ_t of DPCM versus coupling strength γL. Solid line is the theoretical calculation. Squares are experimental results. Notice the dimensions of the response time of the theoretical and experimental results are different.
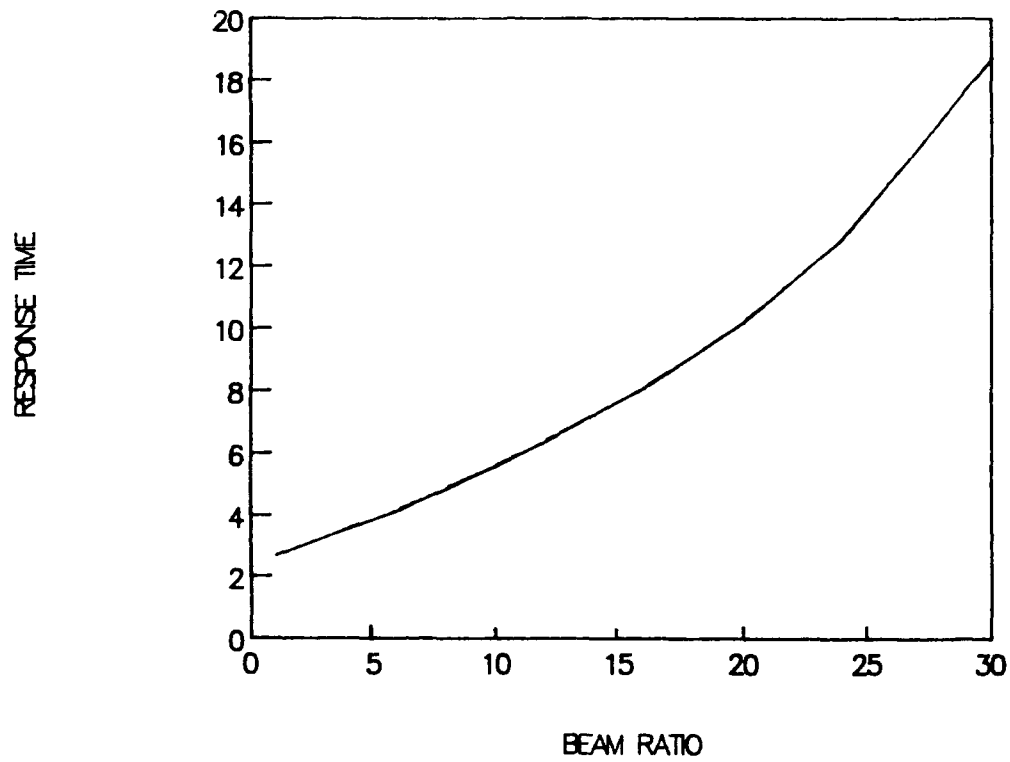
Figure 4.3 — Response time Γ_t of DPCM versus the beam ratio q.
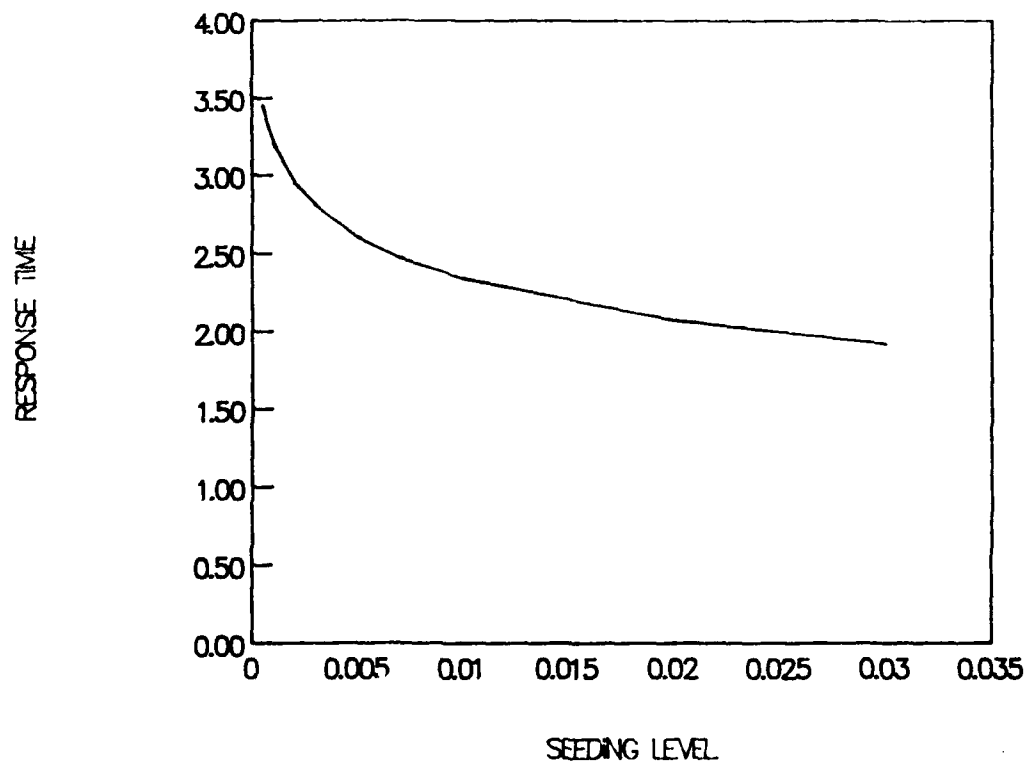
Figure 4.4 — Response time Γ_t of DPCM versus the "seeding" coefficient ϵ.
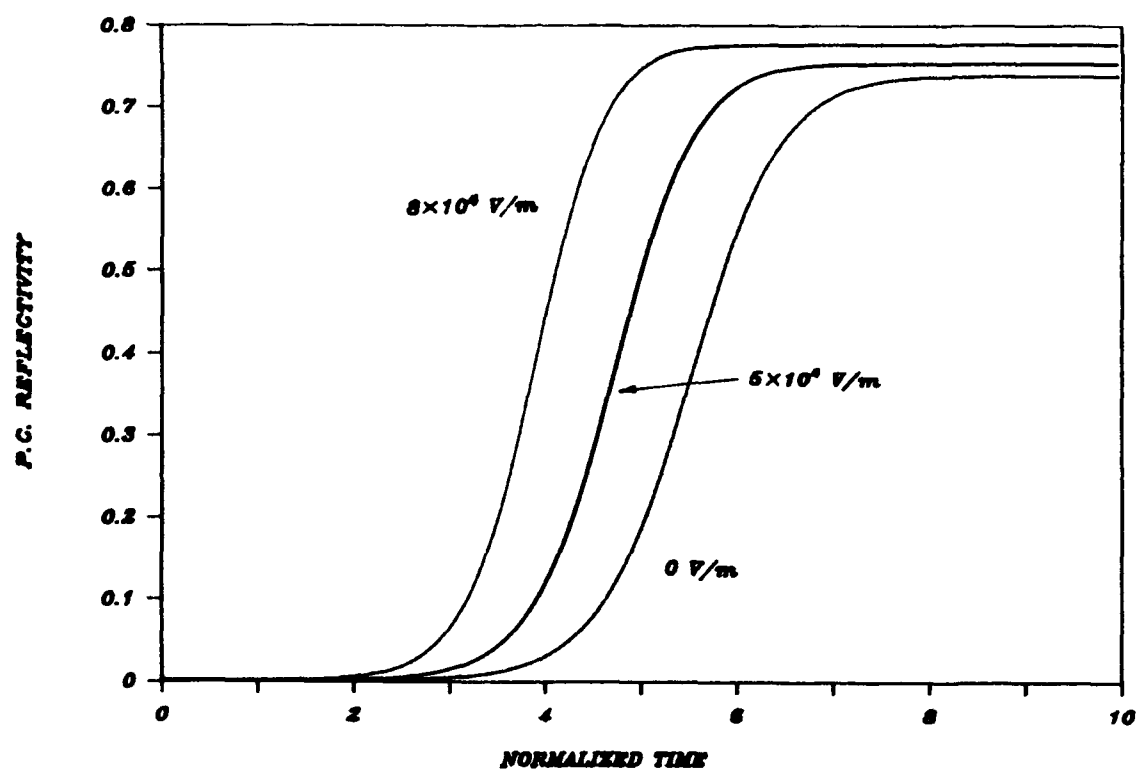
Figure 4.5 — Calculated transient build up of DPCM under various external electric fields, E_0.
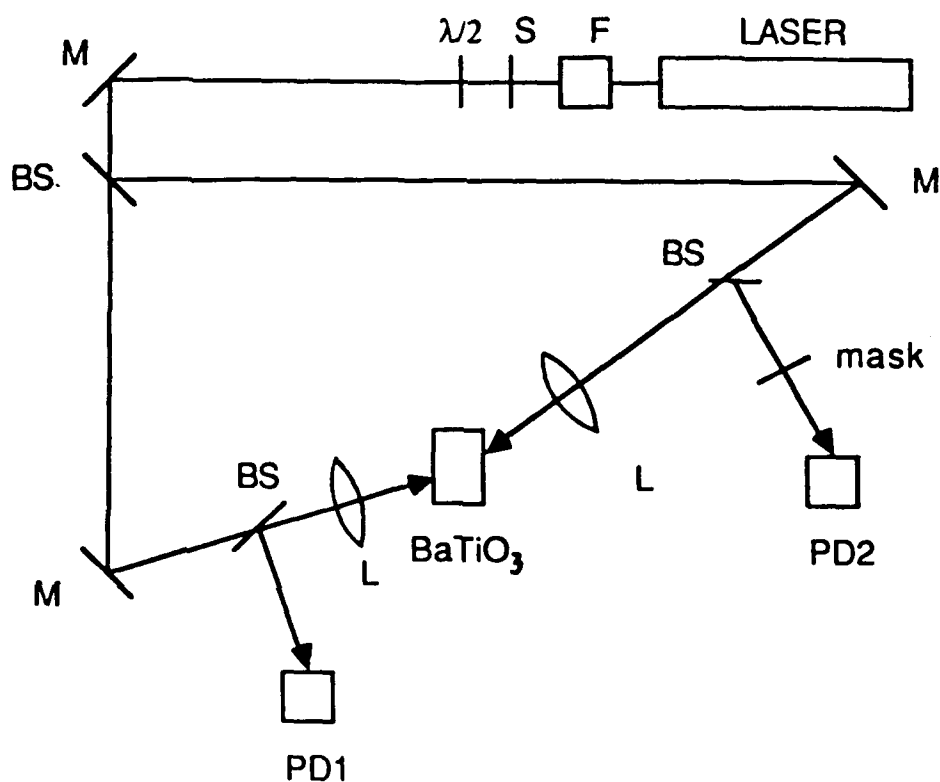
Figure 4.6 — Experimental arrangement for studying the transient process of DPCM. BS's, beam splitters; L's, lenses; M's, mirrors; PD's, photodetectors; S, shutter, F, Faraday isolator.
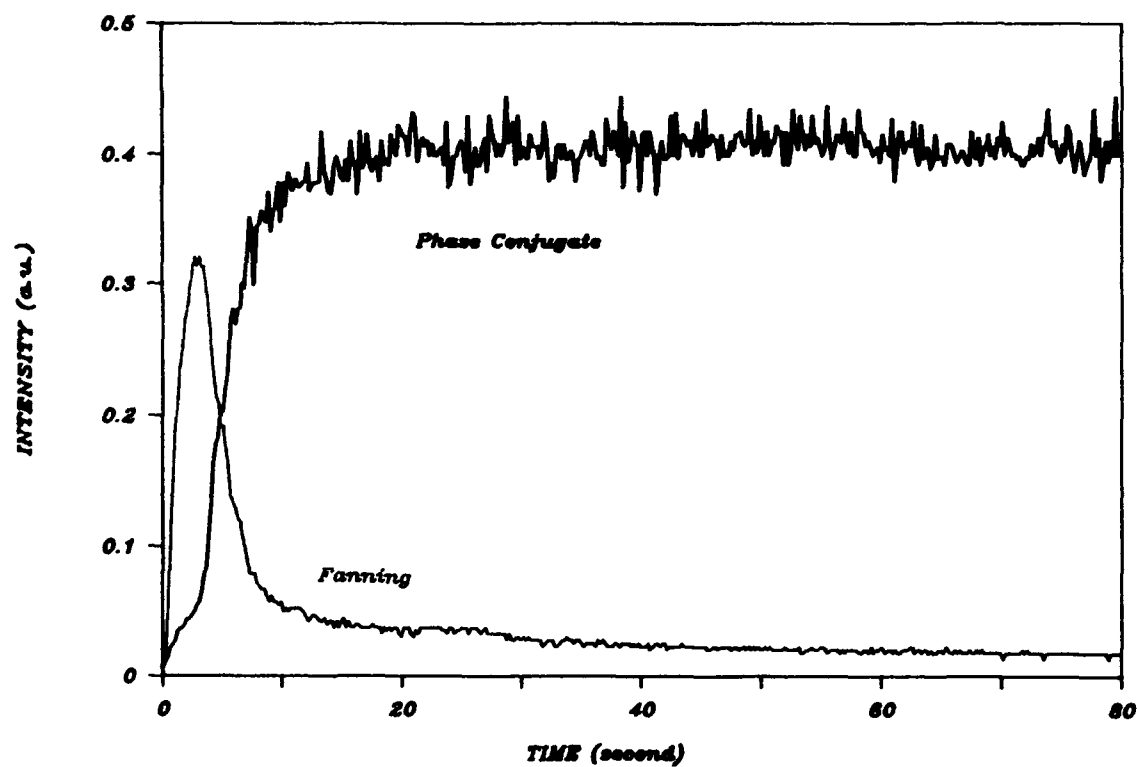
Figure 4.7 — Typical transient process of DPCM measured at $I_0 = 0.82$ W/cm^2, $q = 1$, θ = 62^0. (The absolute magnitudes of the fanning and the phase conjugate are not relevant.)
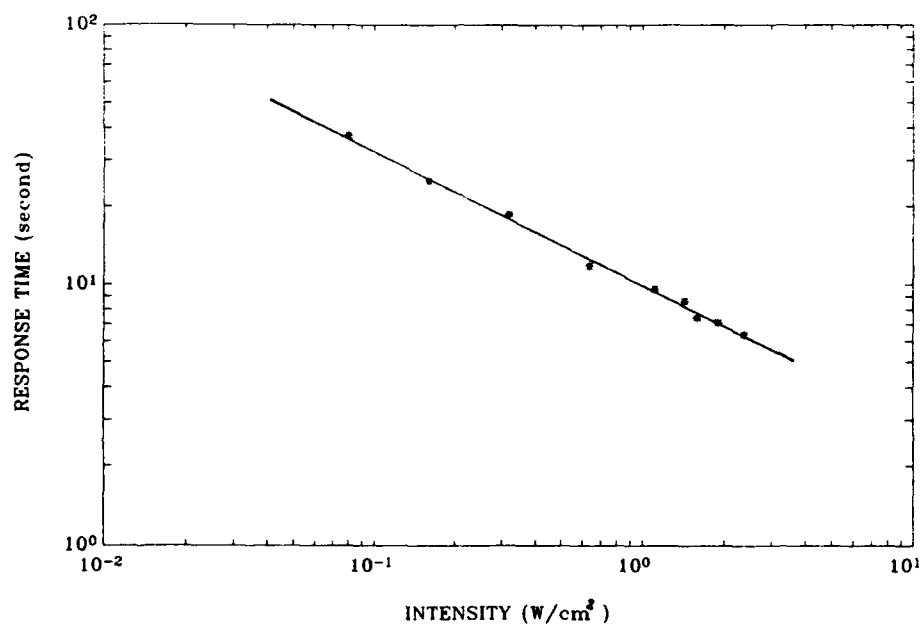
Figure 4.8 — Experimental measurement of the response time Γ_t of DPCM as a function of total intensity at $\theta = 62^0$, $q = 1$.
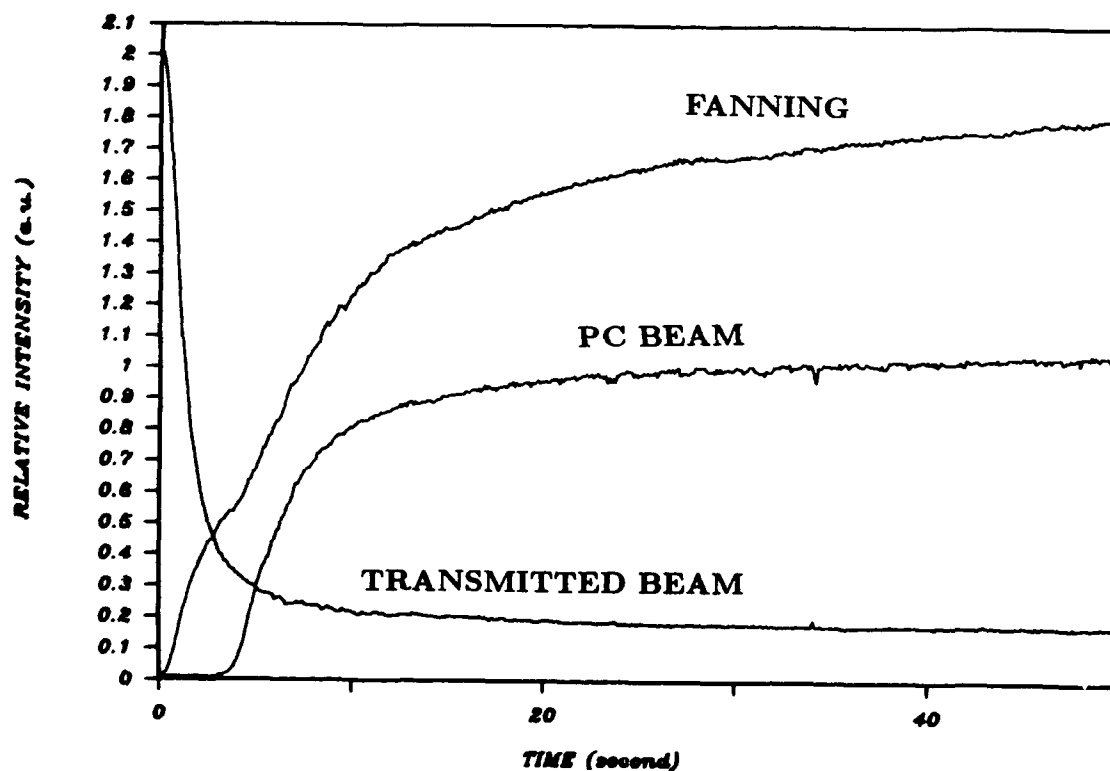
Figure 4.9 — Typical transient proce of SDPCM with total incident power being 12 mc, beam ration $q = 1$, incident ar at 54°. (The absolute ues of each curve are not relevant.)

62
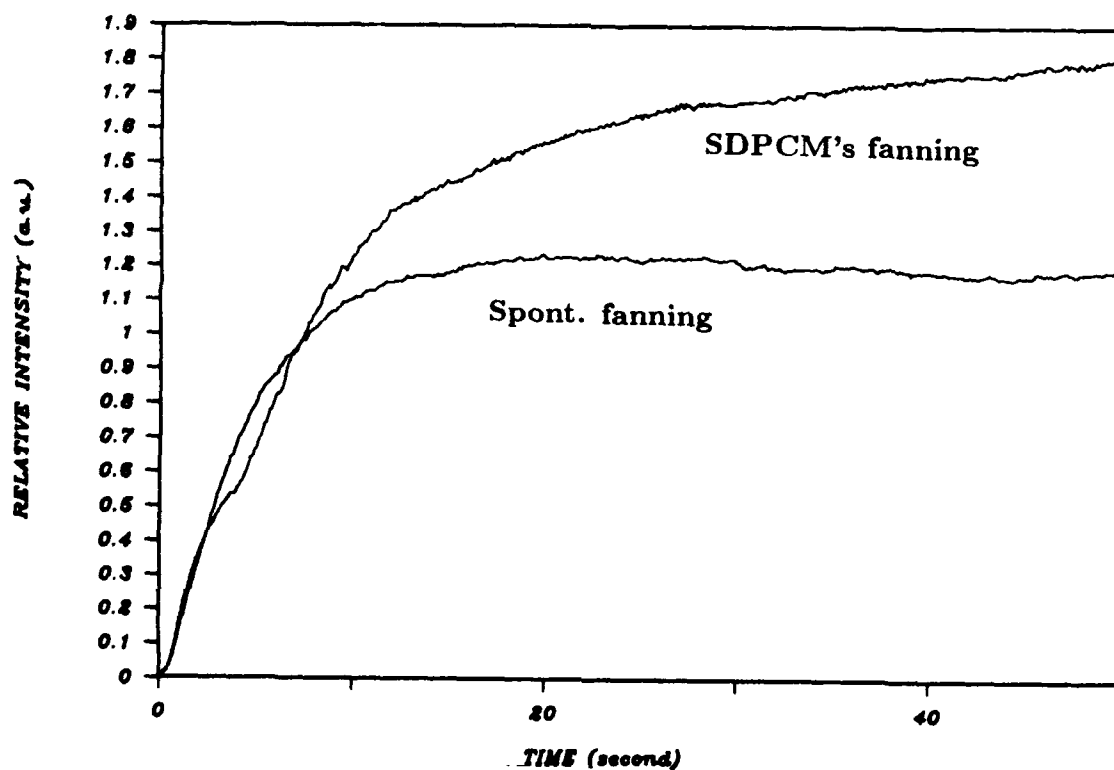
Figure 4.10 — Comparison of the transient process between the spontaneous fanning (i.e., no phase conjugation) and the fanning in the SDPCM. Both transients are recorded by the same photodetector PD_3 at the same place.
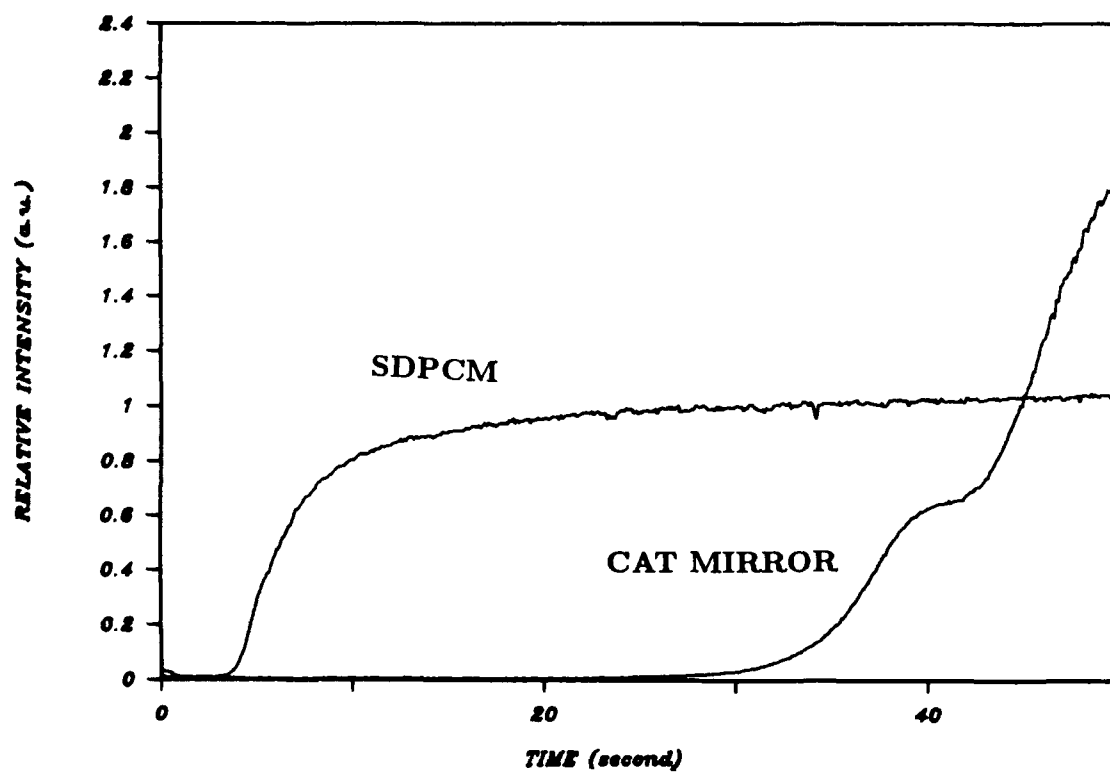
Figure 4.11 — Comparison of the phase conjugate build ups between the SDPCM and the self—pumped phase conjugate mirror of equal incident optical power.
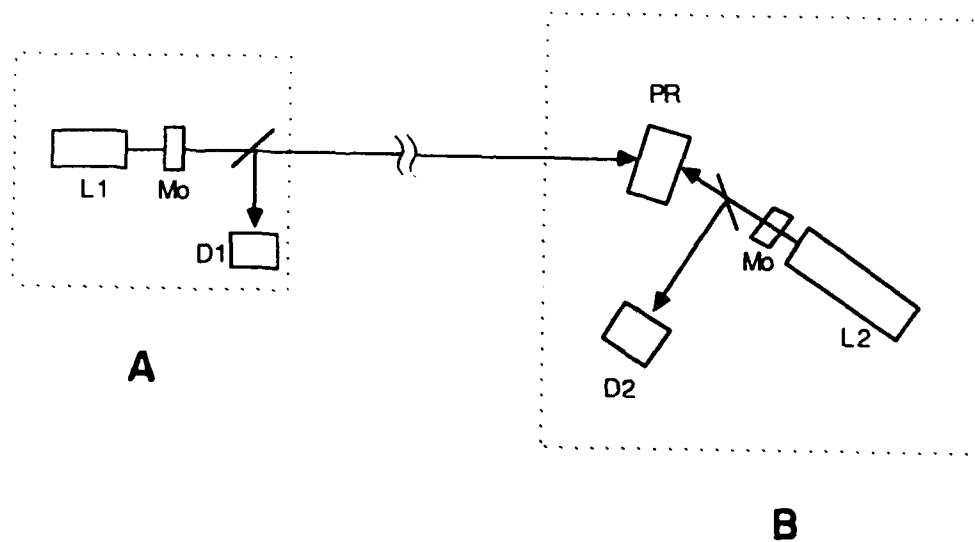
Figure 5.1 — Two—way communication link formed by MPPC.
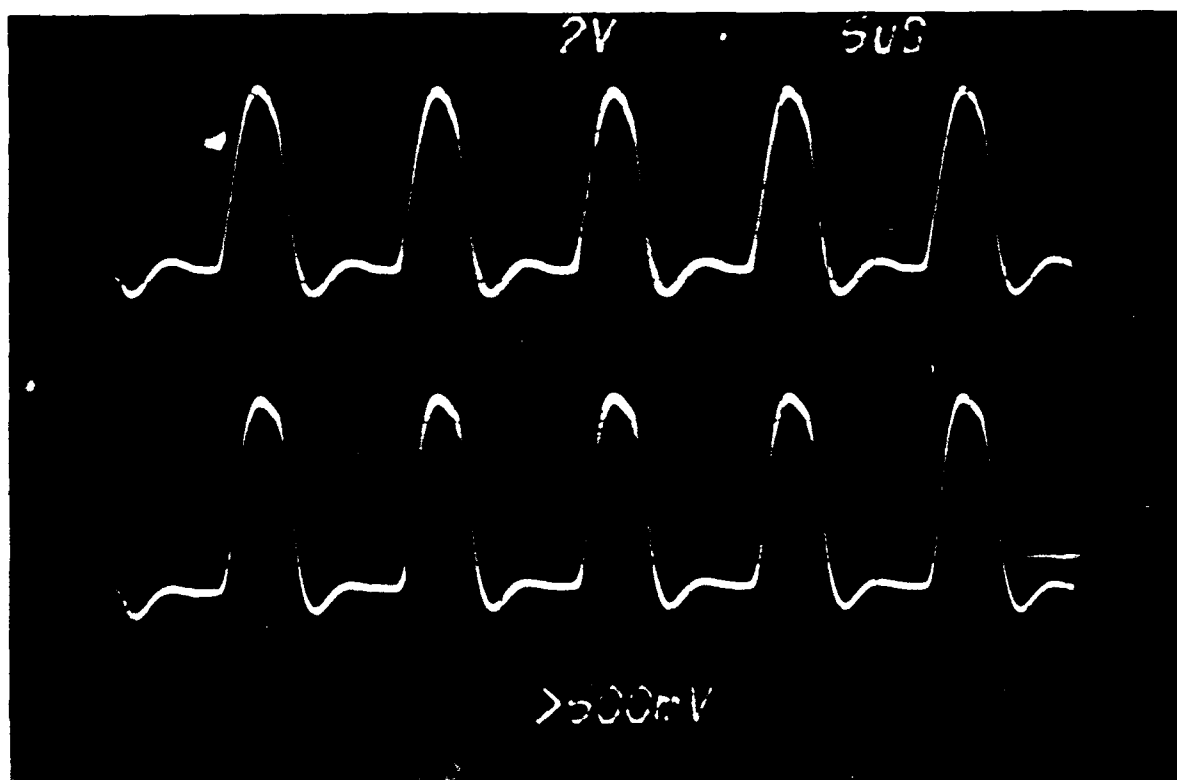
Figure 5.2 — Detected signals of modulated light. The upper trace is the original signal to be transmitted, while lower trace is the signal detected at the receiving station.
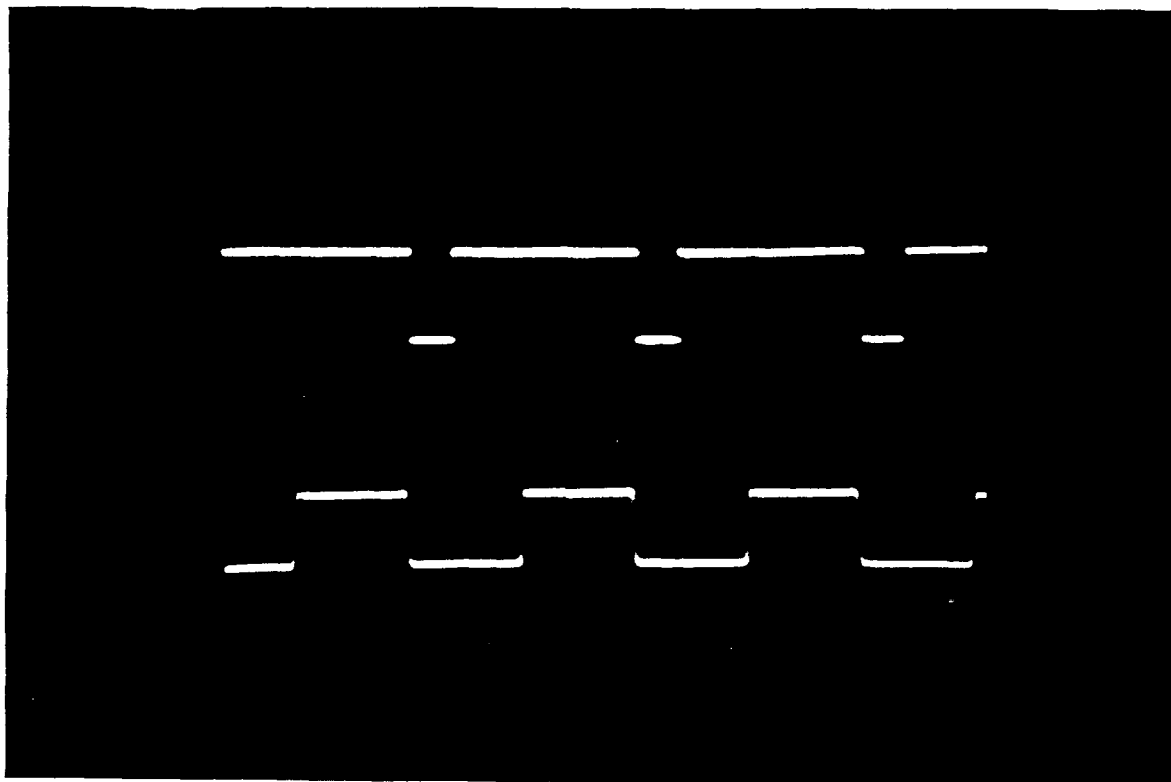
Figure 5.3 — Two—way simultaneous transmission. The upper trace is the signal received at B emitted from A, while lower trace is the signal received at A emitted from B.
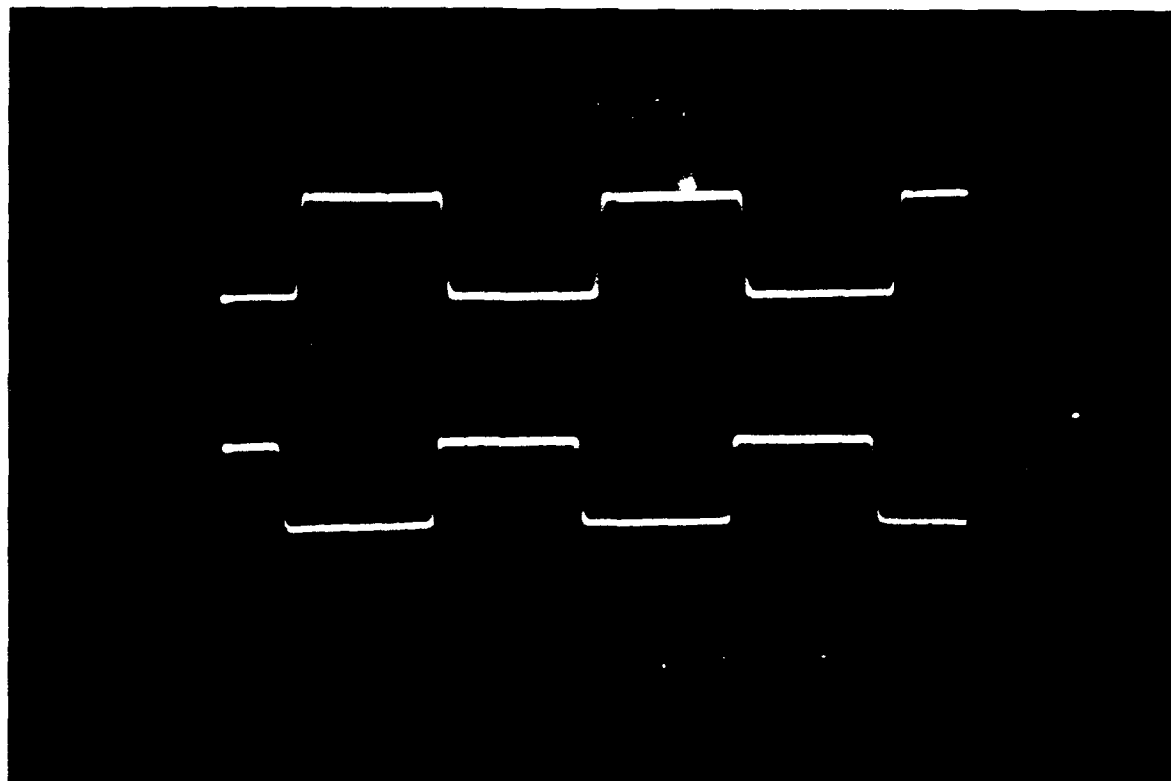
Figure 5.4 — Two—way simultaneous transmission with same modulation frequency but opposite phase.
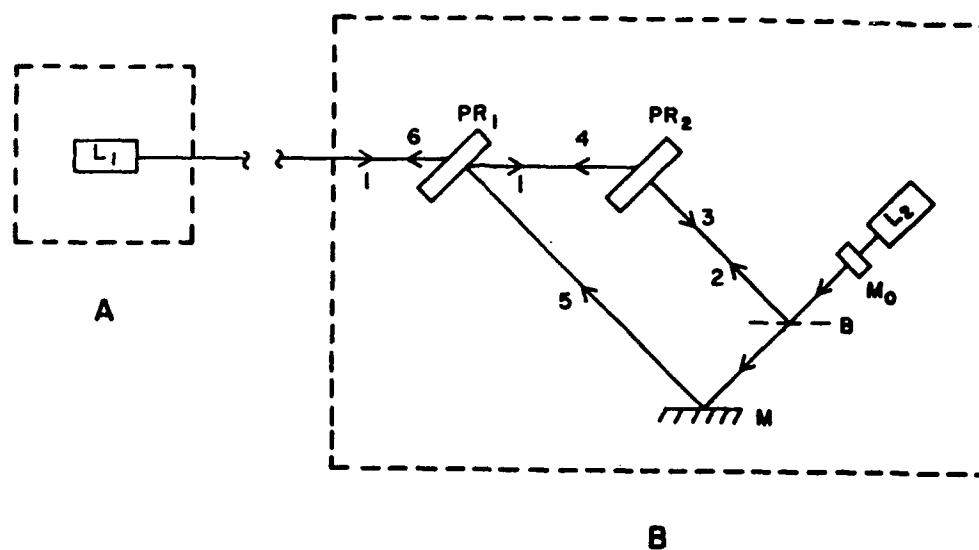
Figure 5.5 — Amplified phase—conjugated signal transmission. *A* is a receiving station emitting a calling beacon beam, while *B* is the source of information to be conveyed to *A*.
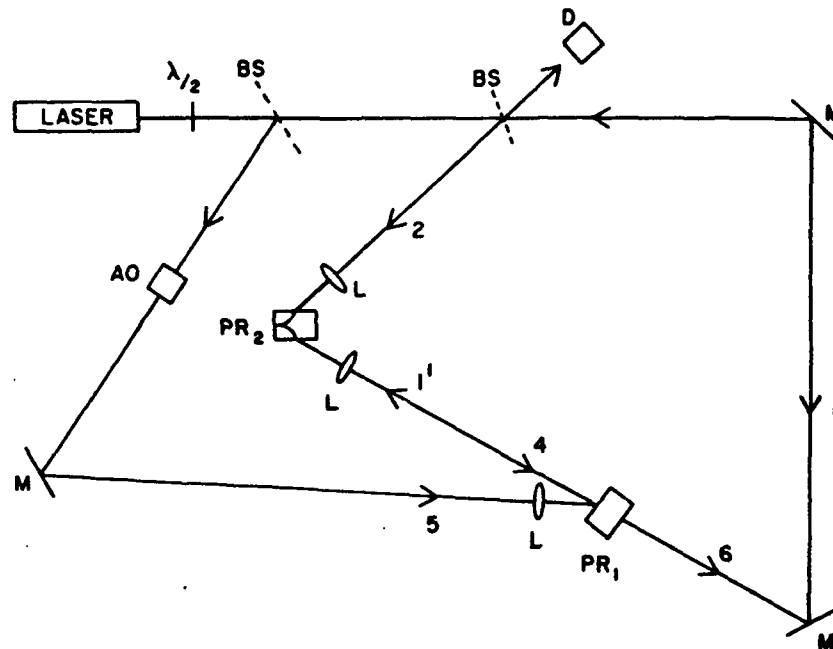
Figure 5.6 — Experimental system containing a multimode argon laser; *BS*, beam splitteers *AO*, acousto–optic modulator; *PR*, $BaTiO_3$, crystals; *M*, mirrors, *D*, photodetectors; *L*, lenses.
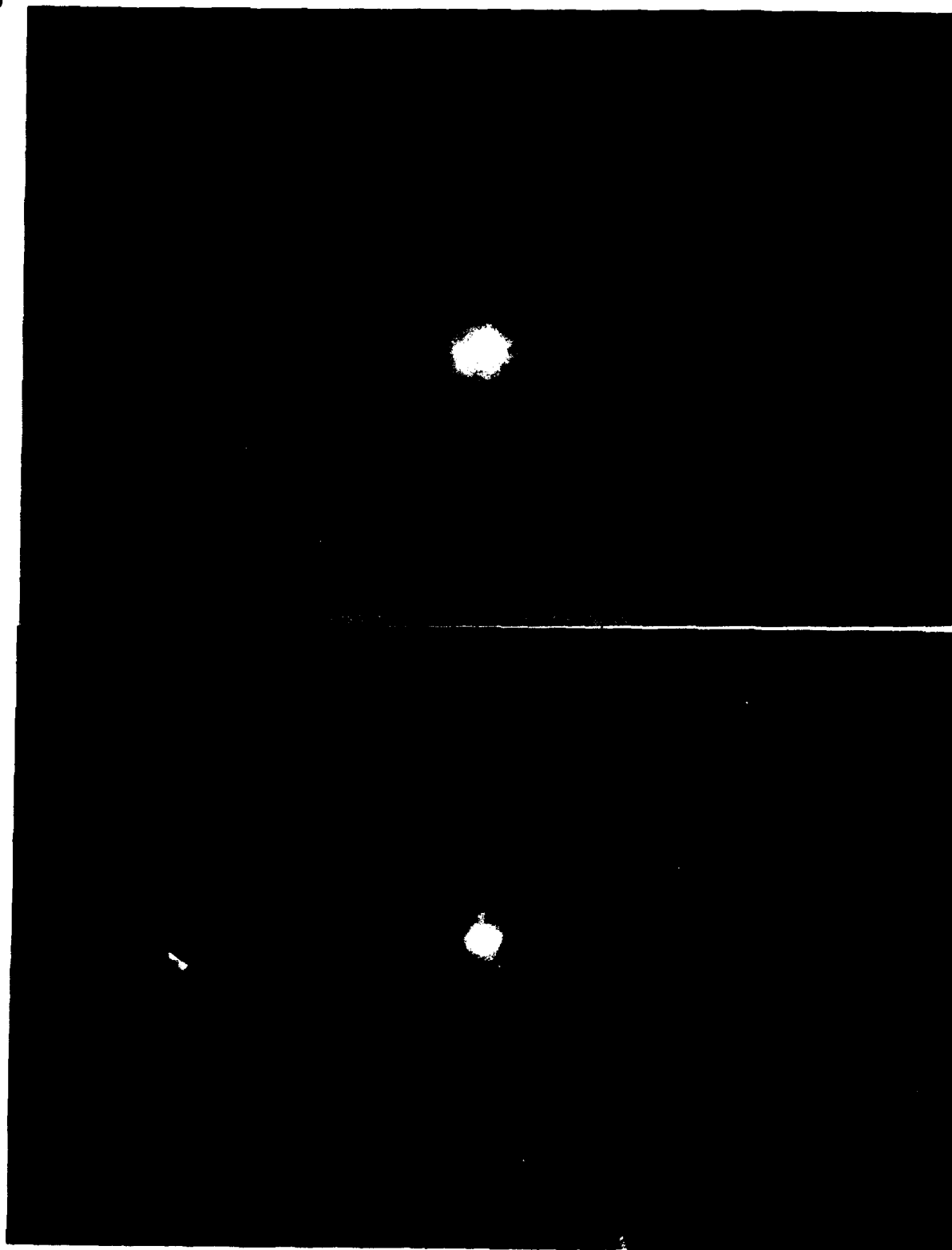
Figure 5.7 — (a) Distorted wavefront after one transit through the distorting medium;
(b) Phase conjugate to the distorted beam after amplification and one transit
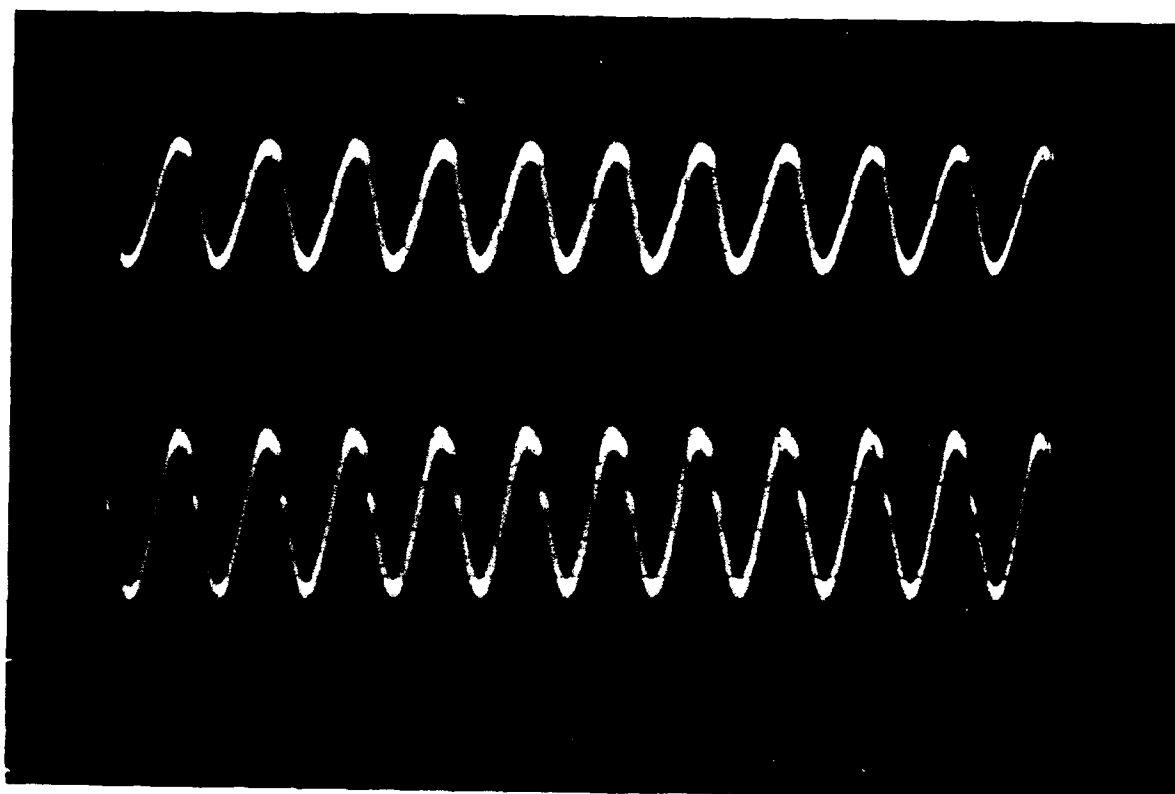rough the distorting medium.

Figure 5.8 — Detected signals for modulated light. The original input signal is on the upper trace, while the amplified signal is on the lower trace. (The voltages presented are not relevant due to the difference between the detection systems.)
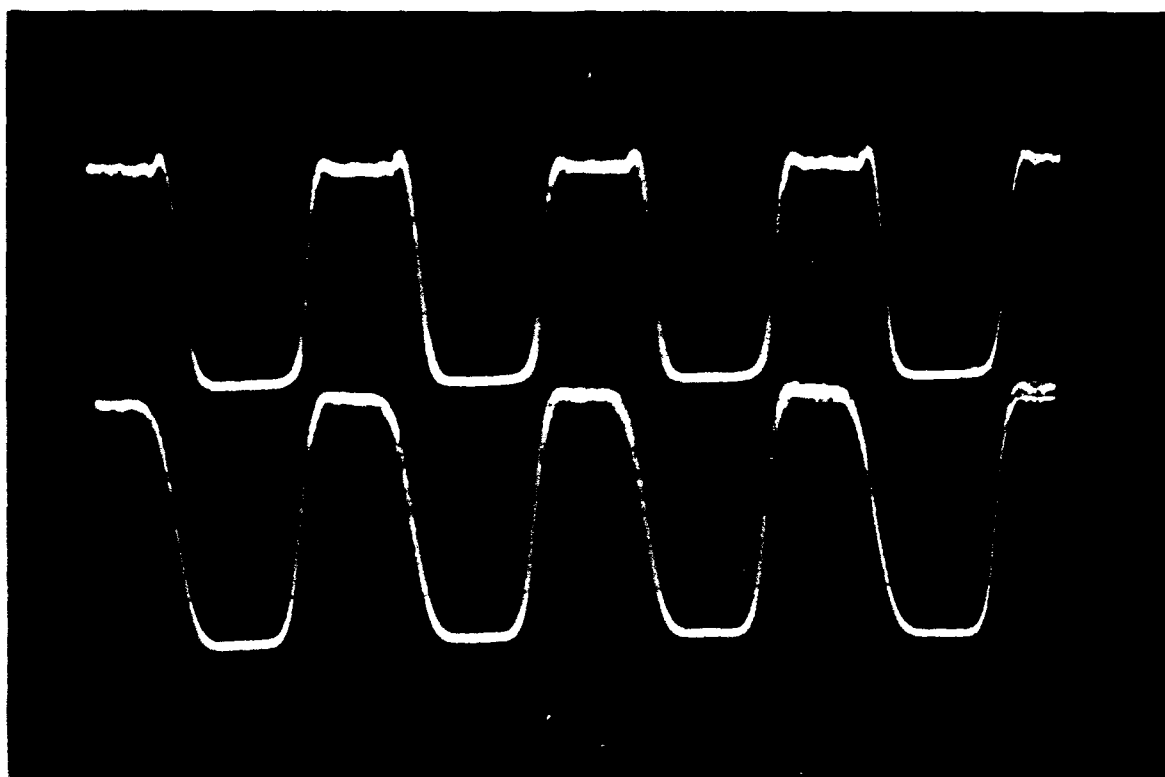
Figure 5.9 — Same as Figure (5.8) but with a mechanical chopper as modulator.
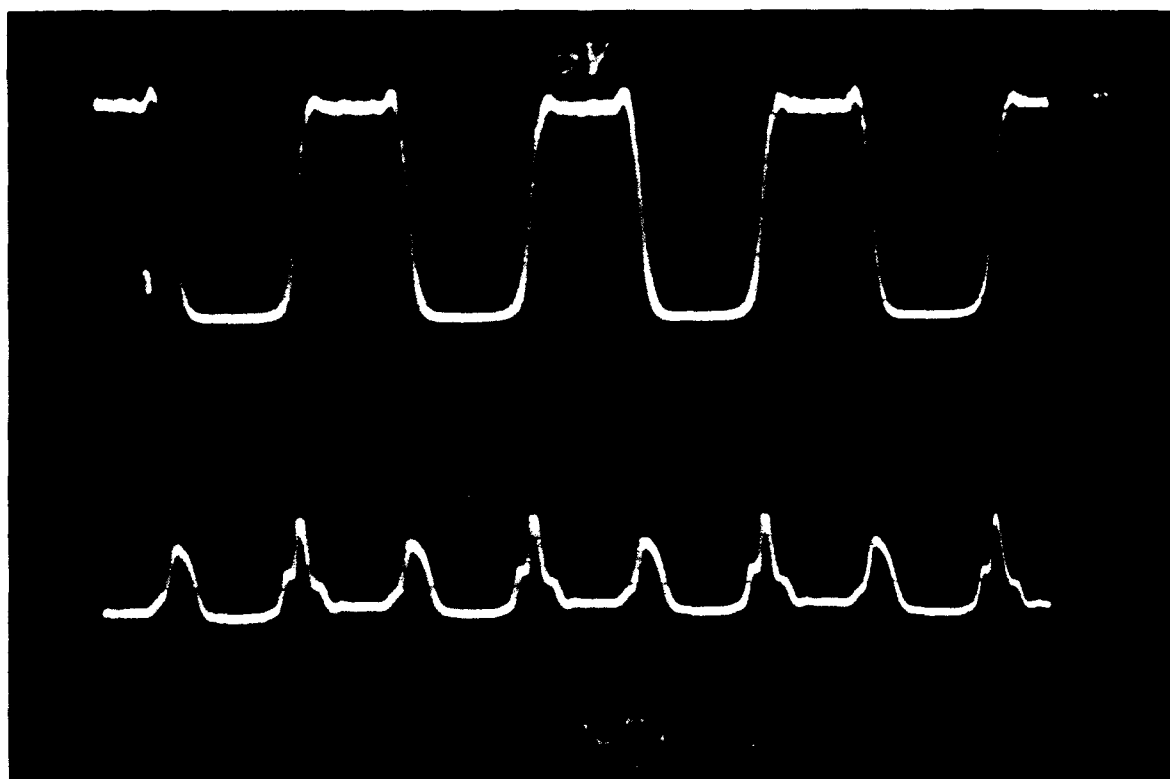
Figure 5.10 — Upper trace as before, but the lower trace is the signal from the edge of the beam.
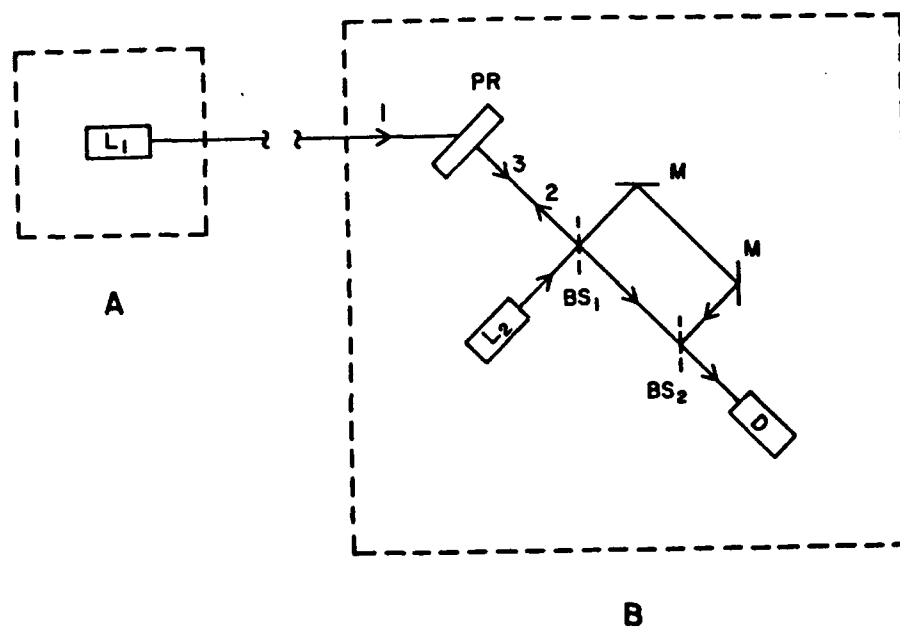
Figure 5.11 — Heterodyne detection system: L_1, laser transmitting station A; and L_2, local oscillator laser at the receiving station B. The local oscillator beam is folded by mirrors M for heterodyne mixing in beam splitter BS_2.

(b)

Figure 5.12 — Interference pattern in a homodyne detector system.
(a) Interference pattern with a distorted beam
(b) Signal interference fringe obtained with beam correction.

MISSION

of

Rome Air Development Center

RADC plans and executes research, development, test and selected acquisition programs in support of Command, Control, Communications and Intelligence (C^3I) activities. Technical and engineering support within areas of competence is provided to ESD Program Offices (POs) and other ESD elements to perform effective acquisition of C^3I systems. The areas of technical competence include communications, command and control, battle management information processing, surveillance sensors, intelligence data collection and handling, solid state sciences, electromagnetics, and propagation, and electronic reliability/maintainability and compatibility.